**Title:**

# Pneumococcus suppresses host inflammatory response through COMMD2 mediated NF-κB degradation by aggrephagy

**Authors:** Michael G. Connor[1*], Lisa Sanchez[2], Christine Chevalier[1], Filipe Carvalho[3], Matthew G. Eldridge[1], Thibault Chaze[4], Mariette Matondo[4], Caroline M. Weight[5$], Sara Dufour[6], Francis Impens[6], Sebastian Baumgarten[7], Jost Enninga[2], Melanie A. Hamon[1*].

**Affiliations:**

1 Chromatin and Infection, Institut Pasteur, Paris, France.

2 Dynamics of Host–Pathogen, Interactions Unit, Institut Pasteur, & UMR CNRS, Paris, France.

3 Institut MICALIS (UMR 1319) INRAE, AgroParisTech, Université Paris-Saclay

4 Institut Pasteur, Université de Paris Cité, CNRS UAR2024, Proteomics Platform, Mass Spectrometry for Biology Unit, 75015 Paris, France.

5 Division of Infection and Immunity, University College London, London, UK.

6 VIB-UGent Center for Medical Biotechnology, VIB Proteomics Core, VIB, Department for Biomolecular Medicine, Ghent University, Ghent, Belgium.

7 Institut Pasteur, Université Paris Cité, Parasite RNA Biology, F-75015 Paris, France

[$] Present address Lecturer in Biomedical and Life Sciences at Lancaster University

*Correspondence:

Michael G. Connor (mconnor@pasteur.fr) & Melanie A. Hamon (melanie.hamon@pasteur.fr)

**Abstract:**

NF-κB driven cellular immunity is essential for both pro- and anti-inflammatory responses to microbes, which makes it one of the most frequently targeted pathways by bacteria during pathogenesis. How NF-κB tunes the epithelial response to *Streptococcus pneumoniae* across the spectrum of commensal to pathogenic outcomes is not fully understood. In this study, we compare a commensal-like 6B ST90 strain to an invasive TIGR4 isolate and demonstrate that TIGR4 both blunts and antagonizes NF-κB activation. We identified, through comparative mass spectrometry of the p65 interactome, that the 6B ST90 isolate drives a non-canonical NF-κB RelB cascade, whereas TIGR4 induces p65 degradation though aggrephagy. Mechanistically, TIGR4 challenge triggers a novel interaction of COMMD2 with p65 and p62. This complex mediates export of p65 for degradation and is necessary for repressing host inflammatory transcription. With these results, we reveal for the first time a new bacterial pathogenesis mechanism to repress host inflammatory response though COMMD2 mediated turnover of p65, and present a paradigm for diverging NF-κB responses to pneumococcus.

**Introduction:**

The eukaryotic NF-kappaB family of transcriptional regulators are well documented for their potent ability to drive both pro- and anti-inflammatory cellular immune responses during microbe-host interaction [1-3]. As such, it is also one of the most frequently targeted host pathways during pathogenic infection. Of the three main documented NF-κB activation pathways - canonical, non-canonical and atypical- the canonical cascade is the best documented as triggered and targeted for exploitation by bacteria [4-7].

The canonical pathway consists of NF-κB subunit heterodimers of p65/p50 or homodimers of p65/p65 bound to an inhibitory protein, such as IkBa. NF-κB subunits are normally sequestered in the cytoplasm in an inactive state [8]. Upon sensing of inflammatory molecules, such as cytokines (IL-1β or TNFα), pathogen-associated molecular patterns (PAMPs; i.e. lipopolysaccharide), and danger-associated molecular patterns (DAMPs; i.e. IL-1α or nuclear protein HMGB1) NF-κB subunits are rapidly activated by phosphorylation on serine residues (S536 and S276). Simultaneously, NF-κB dimers are released from their inhibitory IkB proteins and translocated to the nucleus of the cell for additional modification. Ultimately, this process leads to the binding of activated dimers to cognate NF-κB DNA motifs, thereby inducing NF-κB dependent gene transcription. NF-κB activation is tightly controlled for precise and rapid induction, but also for prompt repression. NF-κB dimers can be repressed through extraction, sequestration, and degradation from within the nucleus, while in parallel blocking cytoplasmic activation and promoting transcription of negative regulators [4,5,7,9-13]. However, in contrast to the myriad of studies on activators only a few negative regulators of NF-κB and their pathways have been documented.

COMMD (copper metabolism gene MURR1 domain)[14] proteins are among the select few documented negative regulators of NF-κB [12,14-19]. There are ten members of the COMMD family, all of which, interact with NF-κB to regulate signaling. The best-studied architype member, COMMD1, upon stimulation by TNF will lead to extraction of p65 from chromatin, followed by ubiquitination and proteasomal degradation. This process, functions independently of NF-κB nuclear translocation and IkBa, but through association with Cullin proteins, is able to terminate NF-κB signaling [12,14,16-22]. For the other COMMD proteins, however, neither their functional activity, their mechanism of NF-κB repression, or their interacting partners, outside of cullins, are known.

Unsurprisingly many bacterial species actively target the NF-κB pathway to repress the innate immune defenses of the host and support their survival. To date, all bacterial processes either coopt NF-κB repressors or directly target NF-κB pathway proteins using virulence factors (general review [3,23]). We and others have shown the obligate human pathobiont, *Streptococcus pneumoniae* (the pneumococcus), fine-tunes NF-κB signaling to support its interaction with the host, across the spectrum of commensal to pathogenic outcomes [24-30]. Surprisingly, we showed that a pathogenic *S. pneumoniae* strain showed very little NF-κB signaling compared to a colonizing, asymptomatic strain.

Here, we demonstrate that a pathogenic TIGR4 pneumococcal strain [24], in contrast to a commensal-like 6B ST90 isolate [24], represses phosphorylation and activation of NF-κB p65. In fact, TIGR4 infection leads to specific degradation of p65 in airway epithelial cells, even upon stimulation with a strong inflammatory agonist, IL-1β. We performed an interactome of p65 and show that each pneumococcal strain interacts with diverging p65 interacting partners, revealing an original aggrephagy mechanism involving COMMD2 and p62. Furthermore our studies on the understudied functionality of COMMD2 by RNAi demonstrated it is necessary for TIGR4 repression of host inflammatory cytokine production. Finally deeper investigation of the COMMD2 interactome in comparison to the 6B ST90 isolate and under stimulation with the potent pro-inflammatory cytokine IL-1β revealed further specificity to TIGR4 and COMMD2 enrichment for additional transcriptional and translational components. Altogether, we report a novel mechanism of pathogenesis to degrade p65 and repress the host response that is specifically induced by TIGR4.

**Results:**

TIGR4 antagonizes NF-κB p65 activation.

Previously we showed a commensal-like 6B ST90 pneumococcal strain activated p65 to drive a unique inflammatory signature in comparison to a disease causing TIGR4 strain [24]. In contrast challenge with an invasive TIGR4 strain resulted in decreased transcriptional activation of several inflammatory cytokines [24,31]. This suggested that TIGR4 either disrupted NF-κB activation, or TIGR4 was not engaging NF-κB pathways in airway epithelial cells.

To directly measure NF-κB activation, we challenged A549 cells with either TIGR4 or 6B ST90 alone, or in combination with IL-1β, a pro-inflammatory stimulus known to drive p65 activation, by phosphorylation of the key serine residues 536 and 276 (review [10]). Cells were collected 2hr post-challenge for immunoblotting and the total levels of p65 were determined. Interestingly, upon infection with TIGR4, p65 levels significantly decreased compared to uninfected or 6B infected cells (Fig. 1A & B). It is important to note that p65 levels decreased even in the presence of IL-1β, which normally drives p65 activation.

Regardless of the total level of p65, we also evaluated the activity level of p65 by measuring phosphorylation at S536 and S276, under all conditions. TIGR4 was able to induce phosphorylation at S276, albeit at levels significantly lower than IL-1β alone, or 6B infection, but not at S536 (Fig. 1A, C, D). Importantly, time course monitoring of S536 phosphorylation, reveals that at no time point during infection, do the levels increase above uninfected levels (Sup. Fig. 1A). Taken together, these results show that TIGR4 is a poor activator of p65 in comparison to the 6B ST90 strain. Remarkably, the addition of IL-1β during TIGR4 challenge did not restore phosphorylation of S536 or S276 to levels comparable to IL-1β alone suggesting this strain of pneumococcus is actively antagonizing NF-κB signaling.

*S. pneumoniae* is an opportunistic respiratory pathogen. Thus, upper airway epithelial cells are among the first to be encountered and in turn are initial triggers of the host response to pneumococcus. Therefore, we studied p65 levels and phosphorylation in primary human nasal epithelial cells (Sup. Fig. 1A) and nasopharyngeal Detroit 562 cells (Sup. Fig. 1B). Importantly, both of these cell types display the same blunting of NF-κB activation.

We further evaluated nuclear translocation of p65 by immunofluorescence, as this is a hallmark of p65 activation. Nuclear p65 intensity was quantified and normalized to the nuclear area by segmenting on the DAPI nuclear strain for TIGR4 (+/- IL-1β) against uninfected and IL-1β controls (Fig. 1E & F). In comparison to uninfected conditions, TIGR4 challenge caused slight nuclear recruitment of p65, but remained significantly lower ($pV \leq 0.001$) in comparison to IL-1β alone. Unexpectedly, there was a significant increase in nuclear p65 between TIGR4 + IL-1β and IL-1β alone (Fig. 1E & F), establishing that p65 is translocated in the TIGR4 + IL-1β condition even though phosphorylation levels are aberrant. It should be noted that this increase could be overestimated due to the cellular nucleus shrinking upon infection.

127 We then tested if abnormal activation influenced downstream transcription of p65 dependent
128 genes. Total RNA was collected from A549 cells at 10, 30, 90, and 120 minutes post challenge with
129 TIGR4 (+/- IL-1β) and IL-1β alone. Relative expression was determined for IL-6, IL-8, CFS2 and PTGS2
130 (COX-2) against uninfected/untreated controls at each time point. TIGR4 in comparison with IL-1β
131 alone did not lead to activation of any of the genes out to 2h post challenge, which is in-line with our
132 previous findings [32] (Fig. 2A). Furthermore, under conditions where IL-1β was added during TIGR4
133 challenge, there was both a delay and a repression of these transcripts in comparison to IL-1β alone.
134 This was corroborated with the diminished p65 phosphorylation at S536 at the protein level at the
135 same time points (Sup. Fig. 1A).
136 Transcriptional activation by p65 requires its binding to cognate kappa-binding sites at the
137 chromatin level. Therefore, we evaluated levels of chromatin bound p65 at the locus of the NF-κB
138 dependent gene *PTGS2* and *CSF2* as these two genes had striking transcriptional profiles. Herein,
139 chromatin was collected from A549 cells 2 hrs post-challenge with TIGR4 (+/- IL-1β) and the recovery
140 of p65 quantified against uninfected and IL-1β controls by ChIP-qPCR targeting kappa-binding sites
141 upstream of the *PTGS2* and *CSF2* transcriptional start site (Fig. 2B). For both genes TIGR4 challenged
142 cells resulted in less than 5% recovery of p65. This stands in contrast to the three-fold higher p65
143 recovery in IL-1β alone (Fig. 2C & D). Interestingly, in the TIGR4 + IL-1β condition p65 recovery was
144 comparable to IL-1β alone (Fig. 2C & D), which is in agreement with our previous data showing p65
145 nuclear translocation. Therefore, the lack of p65 driven transcription under TIGR4 challenge is
146 intrinsically due to the absence of p65 at the chromatin. Whereas in a potent inflammatory
147 environment the transcriptional repression suggests differences in p65 capacity to promote
148 transcription.
149 Altogether, these data show the TIGR4 pneumococcal strain antagonizes p65 activation even
150 in the presence of the pro-inflammatory cytokine, IL-1β. This creates a dysfunctional p65 signaling
151 cascade leading to poor downstream activation of p65 dependent transcription.
152
153 <u>A divergent NF-κB p65 interactome supports TIGR4 driven p65 degradation.</u>
154 To begin to understand the NF-κB p65 activation differences and identify potential interacting
155 partners responsible for blunting NF-κB gene transcription between the two pneumococcal isolates
156 we performed mass spectrometry of NF-κB p65 (Fig. 3A). Herein, an A549 GFP-p65 cell line was
157 challenged with either TIGR4 or 6B ST90 and 2 hrs post-challenge GFP-p65 was immunoprecipitated
158 with a matched A549 GFP alone control for mass spectrometry interactome analysis. From the analysis
159 we identified p65 posttranslational modifications, as well as proteins interacting with p65 under the
160 different conditions tested (Sup. Table 1).
161 The interactome data for 6B ST90 showed the sole NF-κB associated target was RelB, a major
162 component of the non-canonical NF-κB pathway. Using whole cell lysates obtained from A549 cells 2
163 hrs post challenge with either 6B ST90 (+/- IL-1β) or TIGR4 (+/- IL-1β) we confirmed that RelB was
164 significantly ($pV \leq 0.001$) elevated during challenge with 6B ST90 (+/- IL-1β) in comparison to both
165 uninfected and TIGR4 (+/- IL-1β; Fig. 3B & C) and associated with p65 by co-immunoprecipitation (Sup.
166 Fig. 2C).
167 In contrast, the TIGR4 challenged p65 mass spectrometry dataset enriched for different NF-
168 κB associated targets. Gene Ontology and KEGG pathway analysis enriched for protein degradation
169 pathways, including proteins such as HDAC6, a p62, and ubiquitin (Sup. Table 1) [33]. Indeed, p62 is a
170 classical receptor of autophagy, HDAC6 an ubiquitin-binding histone deacetylase known to be
171 important in modulating autophagy, and together have been shown to degrade protein aggregates
172 through a process termed aggrephagy [33-35]. Therefore, our proteomic data suggested that p65 could
173 be targeted for degradation through an aggrephagy pathway under TIGR4 infection conditions.
174 To begin testing this hypothesis we probed whole cell lysates obtained from A549 cells 2 hrs
175 post challenge with either 6B ST90 (+/- IL-1β) or TIGR4 (+/- IL-1β) for HDAC6 levels, as HDAC6 is
176 degraded along with its cargo during aggrephagy (Fig. 3B & D). Indeed, only during TIGR4 challenge
177 conditions did total HDAC6 levels decrease in comparison to uninfected, IL-1β alone and 6B ST90

178 groups. We then tested this hypothesis further using known chemical inhibitors to either proteasome
179 or aggrephagy/lysosomal pathways. We treated cells with MG132 (10µM) [36], a general proteasome
180 inhibitor, with Bafilomycin A1 (400nM) [37-39], an inhibitor of the terminal vATPase assembly during
181 aggrephagy/lysosome fusion, or with SAR405 (500nM) [39,40], a PI3K inhibitor of the initiation of
182 aggrephagy pathway, and assessed the levels of p65. Bafilomycin A1 and SAR405 treatments restored
183 levels of p65 during TIGR4 challenge (+/- IL-1β) to comparable levels of uninfected and IL-1β alone
184 (Fig. 3E-H), while MG132 had no effect in restoring p65 levels during TIGR4 challenge (Sup. Fig. 2A).
185 The same trend for Bafilomycin A1 upon p65 levels 2 hrs post-challenge with TIGR4 was observed in
186 primary human nasal epithelial cells (Sup. Fig. 2B). These data, along with the identification of HDAC6
187 and p62 in the p65 interactome strongly suggest that TIGR4 is inducing degradation of p65 through an
188 aggrephagy pathway.
189 We further determined if degradation was restricted to only the p65 subunit or was also
190 impacting the levels of p50, which in a heterodimer with p65 is the primary translocated unit to the
191 nucleus [5]. We immunoprecipitated endogenous p65 from A549 cells challenged with 6B ST90 or TIGR4
192 against uninfected and IL-1β and probed for the p50 subunit. Already in the input, the level of p50 is
193 lower upon infection with TIGR4 compared to 6B ST90, which is also noticeable from the
194 immunoprecipitation (Sup. Fig. 2C). This observation further supports that TIGR4 challenge is targeting
195 NF-κB p65 complex as a whole. Overall, these data demonstrate TIGR4, in contrast to 6B ST90, induces
196 diverging NF-κB p65 signaling cascade that results in: 1) differential protein binding and 2) degradation
197 of p65 through aggrephagy.
198
199 <u>COMMD2 associates with both p65 and p62 and translocates to the nucleus</u>
200 Since aggrephagy primarily occurs in the cellular cytosol we analyzed the p65 interactome
201 data for an additional element that could link degradation with nuclear export. Upon deeper
202 investigation we noted our interactome identified COMMD2 and COMMD4 as among the most highly
203 enriched proteins associating to p65 under TIGR4 infection conditions compared to 6B ST90. All of
204 the COMMD protein family associate with NF-κB subunits, with the archetype member COMMD1
205 being shown to terminate NF-κB signaling through proteasomal degradation via export by exportin 1
206 (CRM1) and displacement from chromatin at kappa-binding sites [16,17,19,21,41]. Of the two COMMD
207 proteins found in our TIGR4 dataset, COMMD2 was previously shown, by ectopic expression, to reside
208 in the cell cytosol and had a higher association with RelA and NF-κB1 [14,22]. Given these previous studies
209 and our data we focused on COMMD2. We hypothesized that COMMD2 through association with p62,
210 could be involved in p65 turnover and thus a link to the aggrephagy pathway.
211 Herein, we generated an A549 GFP-COMMD2 ectopic expression stable cell line, from which
212 GFP-COMMD2 was immunoprecipitated from lysates 2 hrs post-challenge with either 6B ST90 (+/- IL-
213 1β), TIGR4 (+/- IL-1β) or from our uninfected and IL-1β controls. Samples were probed for p65 or p62
214 to detect interaction with COMMD2. Our results show that only under TIGR4 challenge conditions do
215 p65 and p62 interact with COMMD2 (Fig. 4A & B). Furthermore, upon addition of IL-1β, p65 interacts
216 with COMMD2 to even higher levels. Therefore, COMMD2 is a new infection specific interacting
217 partner of p65, making a complex of p65-COMMD2-p62.
218 Although infection with TIGR4 leads to p65 degradation, the small amount left in the cell is
219 nuclear (Fig. 1E). Therefore, to evaluate the cellular localization of the p65-COMMD2-p62 we
220 performed immunofluorescence experiments using the GFP-COMMD2 A549 cell line. Using this cell
221 line, we further determined infection induced effect on p62. The GFP-COMMD2 A549 cell line was
222 challenged with TIGR4 (+/- IL-1β) and compared to uninfected and IL-1β controls, followed by
223 paraformaldehyde fixation and probing for p62. Total p62 levels in the nucleus were determined per
224 cell, by segmentation on the GFP-COMMD2 signal for the cellular cell boundaries and DAPI for the
225 nucleus (Fig. 4C). There was a significant ($pV \leq 0.001$) decrease in total p62 levels for TIGR4 challenged
226 cells (+/- IL-1β) in comparison to both uninfected and IL-1β alone (Fig. 4D), which is expected upon
227 activation of protein degradation pathways. Interestingly, there is a reciprocal increase in the nuclear
228 levels of p62 (Fig. 4E), showing that during TIGR4 challenge there is movement of p62 between the

229 cytoplasm and nuclear compartments in addition to degradation. Moreover, we noticed COMMD2,
230 an otherwise cytoplasmic protein containing two nuclear export signals [34,35,42], was translocated in the
231 nucleus of cells challenged with TIGR4 (+/- IL-1β) (Fig. 4C). Similarly to p62, there was a decrease in
232 total COMMD2 levels, indicative of protein turnover, and an increase of COMMD2 in the nucleus (Fig.
233 4F & G).
234 We confirmed our microscopy observation by performing cell fractionations. We
235 immunoblotted cell fractions obtained from the GFP-COMMD2 stable cell line 2 hrs post-challenge
236 with TIGR4 (+/- IL-1β) as well as from uninfected and IL-1β controls (Fig. 4H & I). Whereas cells treated
237 with IL-1β alone displayed 20% COMMD2 in the nucleus, similar to untreated/uninfected cells, TIGR4
238 (+/- IL-1β) challenge conditions had 80% of COMMD2 consistently nuclear (Fig. 4I). The levels of
239 cytoplasmic COMMD2 under TIGR4 (+/- IL-1β) challenge conditions correspondingly decreased,
240 demonstrating a relocalization of COMMD2. Finally, we tested if the commensal-like strain 6B ST90
241 could also induce COMMD2 nuclear localization. Using cellular fractionation and immunoblotting, we
242 show that 6B ST90 was incapable of triggering nuclear localization of COMMD2 (Sup. Fig.3A), which
243 demonstrates relocalization is TIGR4 specific. Strikingly, upon challenge with TIGR4, we observed
244 perinuclear COMMD2 puncta formation (Fig. 4C). Such puncta of protein aggregates, along with a
245 decrease in p62 levels have previously been described [43-47] and further support our findings that TIGR4
246 is activating aggrephagy during infection.
247 To confirm that COMMD2 and p62 were degraded through the same lysosomal turnover
248 shown for p65 in figure 3E, we treated GFP-COMMD2 cells with Bafilomycin A1 (400nM; pre-treated
249 for 3 hrs) and quantified the total levels of p65, p62 and COMMD2 per cell 2 hrs post-challenge with
250 either IL-1β or TIGR4 (+/- IL-1β; MOI 20) using confocal microscopy. Similarly to figure 3E, TIGR4
251 challenged cells (+/- IL-1β) treated with Bafilomycin A1 displayed an increase in p65, but also
252 COMMD2, and restored p62 levels comparably to uninfected controls (Sup. Fig. 3B - D). Moreover, in
253 contrast to uninfected and IL-1β treated cells there was a significant (pV ≤ 0.0001) increase in both
254 p65 and COMMD2 levels in TIGR4 conditions. Therefore, the COMMD2-p65-p62 complex is being
255 degraded through aggrephagy-mediated turnover upon TIGR4 challenge and is amplified in the
256 presence of the pro-inflammatory stimulus IL-1β.
257
258 <u>COMMD2 exports p65 for lysosomal degradation.</u>
259 From our data we reasoned that aberrantly phosphorylated p65 during TIGR4 challenge lead
260 to nuclear translocation of COMMD2 for facilitating nuclear export of these p65 complexes. This
261 mechanism of action would be similar to the architype family member COMMD1, which binds NF-κB
262 in the nucleus and exports it through CRM1 for degradation [12,22]. Therefore, we tested whether
263 COMMD2 was exported through CRM1 by using the Leptomycin B inhibitor [48]. GFP-COMMD2 cells
264 were treated with Leptomycin B (10 nM), and immunofluorescence was used to image p62 and p65.
265 Strikingly, by blocking nuclear export we observed that COMMD2 was now localized to the nucleus in
266 uninfected and IL-1β treated cells. Similarly, p62 and p65 are relocalized to the nucleus. In fact,
267 COMMD2 and p62 were detected in puncta in the nucleus (Fig. 5A), where p65 was localized (Fig. 5B).
268 Notably, our IL-1β positive pro-inflammatory stimulus control, known to drive nuclear translocation
269 of p65, had a significant (pV ≤ 0.0001) increase in the nuclear level of COMMD2 and p62 in comparison
270 to uninfected cells (Fig. 5C & D). These surprising data suggest that under nuclear export blockage,
271 which occurs with Leptomycin B treatment [48], COMMD2 and p62 are naturally recruited to the nucleus
272 at specific puncta through a defined process.
273 Interestingly, upon challenge with TIGR4, Leptomycin B treated cells displayed higher levels
274 of COMMD2 and p62 accumulation in the nucleus than without treatment (Fig. 5A, C & D). Thus, upon
275 inhibiting nuclear export of COMMD2 and p62, these proteins are no longer being degraded upon
276 infection and accumulate in the nucleus (Fig. 4). Similarly, Leptomycin B inhibition also increased the
277 nuclear p65 levels in all conditions compared to untreated cells (Fig. 5E), and even restored p65 levels
278 to those of cells stimulated with IL-1β alone. Although COMMD2 puncta are observed upon addition
279 of Leptomycin B, the substantial amount of p65 trapped within the nucleus of these cells rendered

280 definitive scoring of puncta and colocalization difficult. Furthermore, under conditions of TIGR4 + IL-
281 1β and Leptomycin B inhibition, we observed a significant (pV ≤ 0.0001) increase in p62 puncta
282 compared to TIGR4 alone (Fig. 5F & G). These data therefore show that without Leptomycin B
283 inhibition upon TIGR4 challenge leads to an active CRM1 dependent export of p65. Altogether, these
284 results imply the COMMD2 complex is exported by CRM1.
285
286 TIGR4 mediated COMMD2 nuclear translocation is dependent on Ply.
287 We show in sup. Fig. 3A that nuclear translocation of COMMD2 does not occur upon 6B ST90
288 challenge, raising the question of which bacterial factors are important for the observed phenotypes.
289 Thus, we tested if COMMD2 relocalization occurred in a capsule dependent manner (Fig. 6A & B).
290 Herein, we challenged our stable cell line with either two 6B serotypes of different sequence type (6B
291 ST90 & 6B ST138), TIGR4, and a capsule mutant of TIGR4 (JW TIGR4ΔCPS) in parallel with its parental
292 wildtype strain (JW TIGR4). Cell were fixed 2 hrs post-challenge and imaged as previously to score the
293 nuclear levels of COMMD2 against uninfected controls. These data showed COMMD2 translocated to
294 comparable levels when cells were challenged with either the JW TIGR4ΔCPS or parental wildtype (JW
295 TIGR4; Fig. 6A). Furthermore serotype matched 6B strains, which differ in sequence type, were
296 phenotypically different with 6B ST138 inducing more COMMD2 translocation compared to
297 uninfected and 6B ST90 (Fig. 6A). From these data, we concluded COMMD2 translocation was not
298 dependent upon capsule, but on another pneumococcal protein.
299 Thus, we tested TIGR4 mutants of Pneumolysin (Ply) and Pyruvate oxidase (SpxB), two major
300 pneumococcal virulence factors we have previously shown to affect host cell signaling at the nuclear
301 level [49-51]. A549 GFP-COMMD2 stable cell line was challenged for 2 hrs with either wildtype TIGR4,
302 TIGR4Δply or TIGR4ΔspxB and the nuclear levels of COMMD2 quantified against uninfected or IL-1β
303 alone. Nuclear COMMD2 levels were measured by deconvoluted epifluorescence, and quantified by
304 measuring signal intensity normalized by nuclear area by segmenting the nucleus using DAPI stain (Fig.
305 6C & D). These data show COMMD2 was found primarily within the cytoplasm of uninfected and IL-β
306 treated cells, and translocated to the nucleus upon TIGR4 challenge. While not statistically significant
307 lower levels and phenotypically distinct nuclear translocation occurred for the *ΔspxB* mutant,
308 indicating that pneumococcal pyruvate oxidase and peroxide production may have a partial role in
309 COMMD2 translocation. However, deletion of the PLY toxin completely abrogated nuclear
310 translocation, indicating that this bacterial factor is essential (Fig. 6C).
311
312 COMMD2 is required for TIGR4 repression of the host response.
313 To date knowledge of COMMD protein interacting partners or biological functions outside of
314 their established interaction with NF-κB subunits suggests they are broadly involved with cellular
315 trafficking, proteasome degradation and transcription [12,18,52,53]. To better define a molecular and
316 biological role for COMMD2 in p65 export and turnover during bacterial challenge we assessed the
317 COMMD2 interactome by mass spectrometry (Fig. 7A-C). For this we immunoprecipitated GFP-
318 COMMD2 from A549 cells 2 hrs post-challenge with either TIGR4, 6B ST90 or our positive
319 inflammatory control IL-1β for comparison against uninfected and GFP negative controls.
320 Remarkably our interactome data clearly supported the specificity of COMMD2 during TIGR4
321 challenge with a 5- and 80-fold higher recovery of significantly enriched interacting partners under the
322 TIGR4 condition compared to 6B ST90 and IL-1β respectively (Fig. 7A-D; sup. Table 3). By cross-
323 comparison of these targets 254 unique proteins were associated with COMMD2 under TIGR4
324 challenge with 92 being also found in our p65 interactome dataset (Fig. 3A; sup. Table 1). From the
325 analysis we also identified a putative COMMD2 posttranslational modification associated with
326 ubiquitination or neddylation at Lysine residue 50. Finally, using Panther ontology protein class
327 analysis of the significant targets obtained from the interactome underscored a unique TIGR4
328 enrichment for host metabolite and protein modifying enzymes as well as proteins associated with
329 translation (Fig. 7E). Altogether, these results showed during TIGR4 challenge COMMD2 function was
330 specific with a potential role in host inflammatory response.

We previously showed during TIGR4 challenge the host gene transcriptional signature was substantially repressed [31,32]. Within this context, we speculated that if COMMD2 was required by TIGR4 to repress NF-κB p65 driven host immune gene transcription, that inhibiting COMMD2 would lead to increased cytokine production. To our knowledge, no direct chemical inhibitors of COMMD2 exist, thus we used RNAi to knockdown COMMD2 and p62 in primary human nasal epithelial cells which resulted in 20% and >70% knockdown respectively (Fig. 8A-C). While total knockdown of COMMD2 was not ideal, it was consistent. Thus we proceeded with bacterial challenge suspecting this minimal reduction in COMMD2, in comparison to p62, would be enough to discern a role for COMMD2 in transcription.

Prior to challenge 72 hrs of RNAi targeting COMMD2 or p62 was conducted in primary human nasal cells. These cells were challenged for 2 hrs with either IL-1β or TIGR4 (+/- IL-1β; MOI 20), with post-challenge supernatants collected for ELISA. At 2 hrs post-challenge there were modest changes in IL-6 and IL-8 cytokine levels as expected for such an early time point (Fig. 8D & E). For both IL-6 and IL-8 total levels were reduced during TIGR4 (+/- IL-1β) challenge in the scrambled siRNA condition in comparison to the match IL-1β group. This is in agreement with our RT-qPCR results showing minimal and delayed transcription of these two genes (Fig. 2A). In contrast to IL-6 where RNAi of COMMD2 and p62 had little effect, the total level of IL-8 increased slightly when these cells were treated with IL-1β or challenged with TIGR4 (+/- IL-1β) in respect to their scrambled control conditions (Fig. 8E). Importantly, in both conditions knockdown of p62 (>70%) had little effect on IL-6 or IL-8 cytokine production suggesting that p62 function was independent of the transcription capacity of the host. Overall, these results suggest that COMMD2 is indeed involved with gene transcription and we suspect larger knockdown of COMMD2 would have more effect. Inhibiting COMMD2 during TIGR4 challenge, even at a mere 20%, was enough to increase IL-8 gene transcription.

**Discussion:**

Cellular inflammatory response is a critical component of the host defense to bacteria. Yet, the molecular processes that fine-tune NF-κB cascades across the range of colonizing to virulent bacteria is poorly understood. We show that an invasive *S. pneumoniae* TIGR4 strain, which causes symptomatic disease in murine models [24], blunts p65 activation and inflammatory gene transcription even in the presence of IL-1β – a potent inflammatory cytokine. This is in contrast to a commensal-like 6B ST90 strain that activates p65 and does not affect IL-1β driven NF-κB signaling [24]. Through mass spectrometry interactome and post-translational modification analysis, we show these two pneumococcal isolates have diverging p65 interacting partners and phosphorylation status. The 6B ST90 strain upregulates RelB, a hallmark of non-canonical NF-κB signaling, whereas the p65 interactome for the invasive TIGR4 strain enriched for aggrephagy pathway components. We reveal that p65 is being degraded through a unique TIGR4 induced interaction of COMMD2 with p65 and p62. Our investigation of the COMMD2 interactome identified interacting partners associated with enzymatic activity and gene translation. Altogether, this is the first demonstration of a bacterial pathogenesis mechanism to repress inflammatory gene transcription through targeted degradation of NF-κB p65.

Negative regulation of NF-κB signaling, in contrast to the breadth of knowledge on activatory mechanisms, is poorly documented. This is in part due to the lack of identified targets and mechanisms responsible for attenuating this signaling cascade. Of the known negative regulators, A20 (TNAIP3) and COMMD1 are the better described with the studies using cytokine stimulation. Pointedly neither of these proteins were found in our TIGR4 p65 interactome, which suggests that COMMD2 recruitment during bacterial infection is specific. A20 is primarily a deubiquitinase whose transcription is NF-κB activation dependent. A20 functions in a negative feedback loop to deubiquintinate NEMO, which results in its stabilization with the IKK complex to restore NF-κB sequestration in the cytoplasm. This ultimately terminates the downstream canonical NF-κB signaling cascade of inflammatory response [5,12,54]. In contrast, COMMD1 transcription is NF-κB independent, and facilitates p65 termination by CRM1 mediated export and translocation of p65 to the proteasome for degradation

382 via complex formation of COMMD1 with Elongins B & C, Cullin2 and SOCS1 ($ECS^{SOCS1}$) [14,16,17,19,21,22]. In
383 parallel, COMMD1 contributes to repression of p65 driven gene transcription by occupying the
384 formerly p65 bound kappa-binding site at specific gene promoters [20]. It was put forth that the diversity
385 of potential COMMD, NF-κB and cullin assemblies and the array of physiological stimuli activating such
386 complex formations positioned this family of proteins as powerful selective negative regulators of NF-
387 κB signaling.
388 To date our work is the first to show that COMMD2 mediates p65 turnover through p62 and
389 aggrephagy while simultaneously repressing host NF-κB gene transcription. TIGR4 bacterial challenge
390 is the only stimulus to trigger COMMD2-p62-p65 complex formation, with the functional role of
391 COMMD2 on aggrephagy and host transcription being distinct as neither 6B ST90 nor IL-1β induced
392 comparable interactome. We show that COMMD2 nuclear translocation was independent of the
393 TIGR4 capsule, but dependent on a tandem function of Pneumolysin (Ply) and Pyruvate oxidase (SpxB),
394 as a ΔPly mutant shows no COMMD2 nuclear accumulation, but a ΔSpxB mutant induced partial
395 COMMD2 translocation with a distinct phenotype. These data could indicate that pneumolysin
396 functions as a conduit allowing hydrogen peroxide, or other unknown factors, to enter the host cell
397 for the COMMD2 phenotype. Moreover, given our comparison of two serotype 6B isolates varying in
398 sequence type resulted in different COMMD2 nuclear amounts we propose that pneumococcal
399 isolates of different genomic lineages may regulate expression of virulence factors differently in the
400 presence of host cells.
401 The COMMD2 negative feedback loop on p65 that we uncover here may represent, even in a
402 cellular state without bacterial infection, a precise mechanism to terminate or shift a given p65
403 dependent transcription repertoire. Additionally, by lowering the amount of p65 protein present
404 through degradation, a lower threshold of inhibitory IKK proteins would be needed to quench this
405 cascade within the cell. This could rapidly shift the balance in favor of IKK proteins sequestering p65,
406 and perhaps even favor a switch in NF-κB heterodimers, leading to activation of a different
407 transcriptional repertoire. In essence, such inhibition would be quite potent, as inflammatory
408 transcription, inflammatory signal sensing, and negative inflammatory feedback are all blocked
409 simultaneously. Such a mechanism would greatly favor pathogenic infection and host cell exploitation,
410 as we observe upon TIGR4 challenge. On the other end of the virulence spectrum, the commensal like
411 6B ST90 strain lead activation of the non-canonical NF-κB RelB pathway. Interestingly in the 6B ST90
412 p65 interactome COMMD6 was the only COMMD protein found. Altogether, this suggests that NF-κB
413 subunit association with COMMD protein(s) is stimulus dependent and these partners are possibly
414 strong influencers of how the NF-κB transcription factor family participates in transcription and (or)
415 chromatin binding. Therefore, such interactome studies, in combination with pro-inflammatory
416 stimulus, will reveal new partners that govern p65 regulation.
417 Given the vast array of post-translational modifications on p65 and other NF-κB subunits
418 across differential stimulations has given rise to the "NF-κB barcode hypothesis", which suggests that
419 distinct patterns are linked to how inflammatory gene transcription occurs [55,56]. Supporting this is our
420 exploratory mass spectrometry of p65 phosphorylation, which identified serine 45 (S45) as the only
421 enriched phosphorylated mark during TIGR4 challenge. This mark has previously been shown to
422 negatively regulate p65, although the mechanism is unknown [57]. Lanucara et al., showed that a
423 phosphomimetic mutant of S45 prevented IL-6 transcription and p65 binding to the IL-6 promoter
424 after 3 hours of TNFα stimulation [57]. It remains to be evaluated how this modification affects
425 COMMD2-p62 degradation of p65 or upon repressing p65 host transcription. Notably our previous
426 studies showed TIGR4 challenge induces de-phosphorylation of histone H3 serine 10, which is an
427 essential histone modification associated with inflammatory gene transcription [31,58]. Understanding
428 how this event relates to p65 turnover and COMMD2 may shed light on essential chromatin
429 remodeling dynamics needed to precisely regulate NF-κB p65 DNA binding, extraction and
430 transcription termination not only to pneumococci but also under inflammatory stimuli. Excitingly,
431 the commensal-like 6B ST90 does not induce phosphorylation of this S45 residue. Instead, this strain
432 leads to phosphorylation on S203 in addition to S536 and S276. These marks may be critical for the

433 upregulation of RelB, and (or) the histone demethylase KDM6B, which we previously showed was
434 required for bacterial containment in the upper respiratory tract [24]. Future investigations here may be
435 the best positioned to decipher outstanding questions on how bacteria engage the non-canonical NF-
436 κB pathway and how KDM6B is selectively recruited to gene targets during bacterial infection.
437 Whether differential phosphorylation of p65 is the determining factor in the host response to different
438 strains of pneumococcus remains to be determined. It is tempting to speculate that posttranslational
439 modifications of p65 could represent markers of either host response to commensal or to invasive
440 bacteria.
441 Tuning NF-κB dependent immune gene transcription is fundamental for cellular immune
442 processes of airway epithelial cells exposed to pneumococcus [25,59]. The pro-inflammatory cytokines,
443 TNF-α and IL-1β, are major cytokines necessary for neutrophil recruitment and are found in
444 bronchoalveolar lavage fluid of animals challenged with pneumococcal isolates [25,59,60]. However, a
445 study showed that isolated murine lung epithelial cells exposed to serotypes 19 and 3 failed to induce
446 p65 (RelA) nuclear translocation in comparison to TNFα and IL-1β cytokine treatment alone [25]. Our
447 studies directly address this paradox showing that the invasive TIGR4 pneumococcal isolate is actively
448 engaged in repressing p65 signaling through degradation even in an environment containing pro-
449 inflammatory stimuli. We propose that pneumococcus interaction with the 'primary' contacted host
450 epithelial cell results in repressed NF-κB signaling with simultaneous prevention of negative feedback
451 upon this inflammatory response. However, what has been shown during respiratory infection with
452 other microbes [61,62], is that a balance is needed between pro-inflammatory responses and negative
453 regulation to ensure minimal tissue damage from the influx of neutrophils into the airway tissues [60].
454 Airway epithelial cells play a crucial role in both situations by regulating neutrophil recruitment and
455 promoting epithelial repair pathways leading to tissue resilience and resolution of inflammation
456 [59,60,63,64]. With pneumococci actively antagonizing the ability of airway epithelial cells to both induce
457 and respond to IL-1β we hypothesize an amplifying and runaway inflammatory cascade is created in
458 latter stages of infection where neutrophil influx is detrimental [59,64,65]. This could lead to exacerbated
459 and severe pneumonia with excessive tissue damage allowing pneumococcus to transmigrate through
460 the lungs and into deeper tissues. We put forth that COMMD2, or combinations of COMMD proteins
461 are potent modulators of bacterial driven inflammatory processes, and may represent a novel
462 therapeutic target to avoid runaway inflammation.
463 In conclusion, our study shows a new regulatory role for COMMD2 in restraining p65 through
464 aggrephagy mediated turnover triggered by bacterial interaction. We reveal this process to be specific
465 to invasive pneumococcal challenge and partially depend on pneumolysin. Further studies
466 characterizing both the p65 and COMMD2 interactome under bacterial challenge with isolates
467 representing divergent pneumococcal host interaction may identify new processes exploited at the
468 microbe-host interface to regulate NF-κB signaling and identify novel negative regulators of
469 inflammation.
470
471 **Materials and methods:**
472 Bacteria strains, growth, and enumeration. Serotype 6B ST90 CC156 lineage F (ST90; CNRP# 43494)
473 and TIGR4 were obtained from the Centre National de Référence des Pneumocoques (Emmanuelle
474 Varon; Paris, France) and (Thomas Kohler, Universität Greifswald) respectively. Experimental starters
475 were made from master glycerol stocks struck on 5% Columbia blood agar plates (Biomerieux Ref#
476 43041) and grown overnight at 37°C with 5% $CO_2$ prior to outgrowth in Todd-Hewitt (BD) broth
477 supplemented with 50 mM HEPES (Sigma) (TH+H) as previously described [24]. Inocula were prepared
478 from frozen experimental stocks grown for 3 – 4 hrs to midlog phase in TH+H at 37°C with 5% $CO_2$ in
479 closed falcon tubes. Bacterial cultures were pelleted at 1,500xg for 10 mins at room temperature (RT),
480 washed in DPBS, and concentrated in 1mL DPBS prior to dilution at desired CFU/mL using 0.6 $OD_{600}$
481 /mL conversion factors in desired cell culture media [24]. Bacterial counts were determined by serial
482 dilution plating on 5% Columbia blood agar plates and grown overnight at 37°C with 5% $CO_2$.
483

484 Cell culture conditions and in vitro challenge. A549 human epithelial cells (ATCC ref# CCL-185) and
485 A549 stable cell lines were maintained in F12K media (Gibco) supplemented with 1x GlutaMax (Gibco)
486 and 10% heat inactivated fetal calf serum (FCS) at 37°C with 5% $CO_2$. Detroit 562 human
487 nasopharyngeal epithelial cells (ATCC ref# CCL-138) were maintained in DMEM supplemented with 1x
488 sodium pyruvate (Gibco) and 1x GlutaMax (Gibco) 10% heat inactivated FCS. Primary human nasal
489 epithelial cells (HNEpC; PromoCell ref# C-12620; lot# 475Z023) were cultured and maintained in
490 Airway Epithelial Cell Growth Medium (PromoCell ref# C-21060) mixed 1:1 with PneumaCult™-Ex Plus
491 Medium (STEMCELL Technologies cat# 16237380). All cell lines were discarded after passage 15, and
492 HNEpC discarded after passage 4. For challenge studies cells were plated in tissue culture treated
493 plates at $2x10^5$ cells (6well; for 72 hrs), $5x10^4$ cells (24well; for 48 hrs), or $1x10^4$ cells (96well; for 48
494 hrs) [24]. Bacterial inocula (Multiplicity of infection (MOI) 20) were diluted in cell culture media, added
495 to cells, and bacterial-epithelial cell contact synchronized by centrifugation at 200xg for 10 mins at RT.
496 Plates were moved to 37°C with 5% $CO_2$ for 2 hrs and processed as desired for experiment termination.
497 For inhibitor studies, cell culture media was aspirated, and replaced with filter sterilized culture media
498 containing either of the inhibitors MG132 10 µM final concentration (Sigma ref# M7449), Bafilomycin
499 A1 400 nM final concentration (Sigma ref# SML1661) or Leptomycin B 10 nM final concentration
500 (Sigma ref# L2913) for 3 hrs prior to bacterial addition. Human IL-1β (Enzo Life Sciences ref# ALX-522-
501 056) was used at 10 ng/mL final concentration in cell culture media.
502
503 RNA isolation and RT-qPCR. Total RNA isolated and extracted using TRIzol (Life technologies
504 ref#15596-026) method as per manufacturer's recommendations. Recovered RNA (5 µg) was
505 converted to cDNA with Super Script IV as per manufacturer's instructions, diluted to 20 ng/µL in
506 molecular grade water and 1 µL used for Sybr Green reactions as per manufacturer's instructions on
507 a BioRad CFX384 (BioRad). Relative expression was calculated by ΔΔCt method to *GapDH* [66]. RT-PCR
508 primers listed in Sup. Table 2.
509
510 ChIP and ChIP-qPCR. Detailed ChIP buffer components and procedure were completed as previously
511 reported [24]. Briefly, $8x10^6$ A549 cells were cross-linked with 1% formaldehyde at room temperature
512 and quenched with 130 mM glycine. Chromatin was generated from the collected cell pellets by lysis
513 and sonication in chromatin shearing buffer to a size of 200-900bp. ChIP grade antibody to p65 (L8F6)
514 (CST ref #6956) was used at manufacturer's recommended concentrations and bound to DiaMag
515 beads (diagenode ref # C03010021-150) overnight with gentle rotation. Quantified chromatin was
516 diluted to 10 µg per immunoprecipitation and added to antibody bound DiaMag beads overnight with
517 gentle rotation and 8% of input reserved. Beads were washed as previously described [24], and DNA
518 purified using phenol-chloroform extraction followed by isopropanol precipitation. Recovered DNA
519 suspended in molecular grade water was used for Sybr Green reactions (1 µL) on a BioRad CFX384
520 (BioRad). ChIP-qPCR primers (50-150 bp; 60 °C max melt temperature) were designed to span the NF-
521 κB sites of interest within the promoters of *PTGS2* [67]. % recovery was calculated as 2 raised to the
522 adjusted input Ct minus IP Ct multiplied by 100. ChIP qPCR primers listed in Sup. Table 2.
523
524 Plasmids, molecular cloning and stable cell line generation. All plasmids and primers are listed in Sup.
525 Table 2. Routine cloning was carried out by in vivo assembly [68,69]. Briefly, primers were designed with
526 a 15-20 bp overlap to amplify nucleic acid targets using Phusion Plus polymerase (Thermo ref# F630S).
527 Correct sized bands were excised and nucleic acid extracted by "Freeze and squeeze" [70,71]. Herein,
528 0.7% - 1% agarose gel fragments were frozen for 5 mins on dry ice and centrifuged for 15 mins at
529 >21,000 xg with the supernatant collected – the process was completed two additional times.
530 Collected supernatant containing nucleic acid was then purified using phenol-chloroform extraction
531 followed by isopropanol precipitation and suspension in molecular grade water. Collected nucleic acid
532 was quantified spectrophotometrically using a NanoDrop and mixed at 3:2 (vector: insert) in 10 µl and
533 added to chemically competent E. coli MC1061 or DH5α for transformation. After 1 hr incubation on
534 ice bacteria outgrowth was done for 1 hr in Luria-Bertani (BD) prior to selection on LB agar containing

535 desired antibiotic (Sup. Table 2). All plasmids were isolated with the QIAprep Spin Miniprep Kit (Qiagen
536 ref# 27106) and eluted in molecular grade water (endotoxin free) as per manufacturer's instructions.
537 A549 stable cell lines were generated using the transposon-based sleeping beauty system [72,73]. A549
538 cells were plated in tissue culture treated plates at $2x10^5$ cells (6well) one day prior to transfection
539 with 2 µg plasmid DNA + 150 ng SB100 transposase DNA. After transfection, cells were selected with
540 1 mg/mL Geneticin (Thermo ref# 10131035) for 7 days, with media exchanged on days 1, 3, 5 & 7.
541 Selected cells were collected with Trypsin 0.25% EDTA (Thermo ref# 25200056) and two-way serial
542 diluted in a 96 well tissue culture plate for monoclonal selection for another 7 – 14 days with media
543 containing 1 mg/mL Geneticin and exchanged every 2 – 3 days. Selected colonies that were
544 phenotypically bright were mixed and expanded prior to FACS sorting to ensure purity, and uniform
545 expression.
546
547 Immunoblots and quantification. Whole cell lysates were obtained by RIPA lysis (10 mM Tris HCL pH
548 7.5, 150 mM EDTA, 0.1% SDS, 1% Triton X-100 & 1% Deoxycholate) supplemented with inhibitor
549 cocktail (1X PhosSTOP, 10 mM sodium butyrate, 0.2 mM PMSF). Samples combined with 5x with
550 Laemmli buffer [74], sonicated for 5 mins in a ultrasonic water bath, boiled at 98°C (dry bath) for 10 mins
551 and frozen at -20°C. Whole cell lysates were ran on 4 – 20% pre-cast polyacrylamide SDS PAGE gels
552 (BioRad), transferred to PVDF membrane (BioRad TransBlot) and blocked 1 hr in 5% BSA TBST at room
553 temperature. Membranes were probed overnight at 4°C in 5% BSA TBST with primary antibody to p65
554 (CST ref #6956 or CST ref# 8242), p65 phosphorylation at serine 536 (CST ref# 3033), p65
555 phosphorylation at serine 276 (abcam ref# ab183559), NFkB p105 / p50 (abcam ref# ab32360), RelB
556 (abcam ref# ab180127), SQSTM1 / p62 antibody [EPR4844] (abcam ref# ab109012) or actin AC-15
557 monoclonal (Sigma ref# A5441) as per manufacturer's recommendations. COMMD2 immunoblots
558 were blocked for 1 hr at room temperature in 3% milk TBST and probed overnight at 4°C with the
559 primary antibody (Sigma ref# HPA044190) suspended in 3% milk TBST. Appropriate secondary-HRP
560 conjugated antibodies in 5% Milk TBST were incubated for 1 hr at room temperature prior to
561 development with clarity ECL (BioRad) developing reagents with a ChemiDoc Touch (BioRad).
562 Detroit562 immunoblots were developed using Licor Odessey using secondary antibodies at 1:7,500 -
563 Goat anti-rabbit IgG H&L (IRDye 800CW) and goat anti-mouse IgG H&L (IRDye 680RD) from abcam.
564 Band intensity was quantified by Image Lab (BioRad), or using Fiji [75] (Detroit 562 cells) with linear
565 intensity values $log_{10}$ transformed and normalized to actin prior to any additional ratio metric
566 comparisons.
567
568 siRNA and transfection. Primary human nasal cells were seeded at $2x10^4$ cells per well in a 96well plate
569 the day before RNAi transfection. For RNAi 1 µl of 2 µM Silencer Select siRNA stock for either COMMD2
570 (Ambion ID# s27490) or SQSTM1 (p62; Ambion ID# s16961) was diluted with 9 µl Opti-MEM (Thermo
571 cat# 31985062) and mixed with 10 µl of 0.003% (vol/vol) Lipofectamine RNAiMAX (Thermo cat#
572 13778030)/ Opti-MEM. Complexes were formed during 15 min incubation at room temperature prior
573 to 20 µl of mixture added to previously seeded cells. 96well plate was incubated for an additional 72
574 hrs 37°C with 5% $CO_2$ prior to challenge studies.
575
576 Cell fractionation. Fractionation was performed as previously described as previously described [24].
577 Faction lysates were combined with 5x with Laemmli buffer [74], sonicated for 5 mins in a ultrasonic
578 water bath, boiled at 98°C (dry bath) for 10 mins and frozen at -20°C. Samples were ran on either 10%
579 (for GFP-COMMD2) or 12% (for fraction quality controls) polyacrylamide SDS PAGE gels (BioRad),
580 transferred to PVDF membrane (BioRad TransBlot), blocked 1 hr in 5% BSA TBST at room temperature.
581 Primary antibody in 5% BSA TBST to GFP (abcam ref# ab290), GapDH (abcam ref# ab8245), or histone
582 H4 (abcam ref# ab177840) was completed overnight at 4°C. After 3x 10 min washes in TBST
583 appropriate secondary-HRP conjugated antibodies in 5% Milk TBST were incubated for 1 hr at room
584 temperature and developed with a ChemiDoc Touch (BioRad) as described above.
585

586 Immunofluorescence microscopy and Cellprofiler analysis. For microscopy the desired cell line were
587 seeded on acid washed and UV treated coverslips in 24well or 96well plates as described above. Two
588 hours post-challenge media was aspirated, cells washed in DPBS, and fixed with 2.5% PFA for 10 mins
589 at RT. Fixed cells were blocked and permeabilized overnight in 5% BSA 0.5% Tween20 at 4°C. Primary
590 antibody to p65 (CST ref #6956 or CST ref# 8242), COMMD2 (Sigma ref# HPA044190-25UL; only works
591 for immunofluorescence), or p62 (SQSTM1; abcam ref# ab109012) were diluted at 1:1,000 in 5% BSA
592 0.5% Tween20 and incubated overnight at 4°C. Cells were washed 3x 10 mins at RT in PBS + 0.1%
593 Tween20 prior to 1 hr incubation at 1:1,000 dilution of either Alexa Fluor 594 or Alexa Fluor 647
594 secondary antibody. Nuclei were stained with 10 ng/mL final concentration of Hoechst 33342 for 15
595 mins. Coverslips were rinsed in PBS and molecular grade water prior to mounting with Fluoromount-
596 G Mounting Medium (INTERCHIM). Confocal microscopy images were acquired on a Nikon TiE inverted
597 microscope with an integrated Perfect Focus System (TI-ND6-PFS Perfect Focus Unit) and a Yokogawa
598 Confocal Spinning disk Unit (CSU-W1). Nine images per well were acquired using a 20X air objective
599 (NA 0.75) at a step-size of 0.9µm in z-plane. Deconvoluted epifluorescent images were acquired on a
600 Cytation 5 (BioTek) using a 20X air objective (NA 0.75) with a grid of 3 x 3 (9 images en total).
601
602 Images were processed for background using Fiji [75], and segmented using Cell Profiler [76-78]. Briefly, the
603 pipeline for image analysis consisted of sequential modules to 'IdentifyPrimaryObjects' based on
604 channel signal for nuclei (DAPI stain), p65 (Alexa594), or p62 (Alexa594). This was followed by
605 'IdentifySecondaryObjects' for the GFP-COMMD2 signal via propagation of identified nuclei. Objects
606 were related to each other to maintain cohesion between identified nuclei, cell and cellular contents
607 (p65 or p62). For puncta, the additional module, 'EnhanceorSupressFeatures' with 'Speckles', was
608 used. This used a global threshold strategy with Otsu threshold method and a 2% minimum boundary
609 to identify puncta contained within the segmented nuclei.
610
611 Immunoprecipitation. Cells were lysed in 250 µL of RIPA lysis (10 mM Tris HCL pH 7.5, 150 mM EDTA,
612 0.1% SDS, 1% Triton X-100 & 1% Deoxycholate) supplemented with a protease mixture inhibitor
613 (Roche Complete, EDTA free). Lysates were either immunoprecipitated using GFP-trap agarose beads
614 (ChromoTek ref# gta-10) or with slurry protein G beads (Sigma-Aldrich Fast Flow Protein G sepharose).
615 For GFP-p65 and GFP-COMMD2 the samples were immunoprecipitated as per manufacturer's
616 instructions with the elution was recovered in either 5x with Laemmli buffer [74] and boiled at 98°C (dry
617 bath) for 10 mins, or left in Trypsin digest buffer (see LC-MS/MS Mass-spectrometry and analysis). All
618 samples were frozen at -20°C. For endogenous samples the lysates were incubated on a rotating wheel
619 at 4 °C for 20 min before adding 1 mL of dilution buffer (150 mM NaCl and 50 mM Tris-HCl pH 7.5
620 supplemented with Protease mixture inhibitor) to reduce the detergent final concentration below
621 0.1%. The lysates were then centrifuged at 10,000 × g for 10 min, and the insoluble pellet was
622 discarded. For p65 IP the lysates were then incubated with 2 µg of antibody CST ref #6956 or CST ref#
623 8242) at 4 °C for 2 hrs before adding 20 µL of slurry protein G beads (Sigma-Aldrich Fast Flow Protein
624 G sepharose) for 20 min. The beads were then washed before adding 20 µL of Laemmli buffer
625 supplemented with 2% β-mercaptoethanol and boiled for 5 min.
626
627 Cytokine quantification by ELISA. Supernatants we collected from primary nasal epithelial cells seeded
628 in a 96well plate as previously described. For this 200 µl of supernatant per well was collected 2 hrs
629 post-challenge with IL-1β or bacteria, centrifuged in a 96well U-bottom plate for 10 min at 1,500 x g
630 to pellet bacteria and cellular debris. 120 µl of cleared supernatant was collected into a 96well flat
631 bottom plate and frozen at -20°C until use. 25 µl of supernatant was used as per manufacturer's
632 recommendations for ELISA kits measuring human IL-6, and IL-8 (R&D systems cat #s DY206-05, %
633 DY208-05).
634
635 LC-MS/MS Mass-spectrometry and analysis. For label-free quantitative proteomic analysis of GFP-p65
636 and GFP-COMMD2 the respected A549 cell lines were plated in 6well tissue culture plates, and

637 challenged with bacteria for 2hrs as described above. One plate (~$5x10^7$ cells) per condition was
638 harvested using RIPA lysis and immunoperciptated with GFP-trap agarose beads (ChromoTek ref# gta-
639 10) as per manufacturer's instructions. Three or four independent biological replicates were prepared
640 and analyzed for each condition. Prior to on-bead Trypsin digestion, the samples were washed 3x in
641 trypsin digest buffer (20 mM Tris.HCl pH 8.0, 2 mM $CaCl_2$).
642
643 For pull down of GFP-p65 on bead digestion was performed strictly as described by Chromotek. Briefly,
644 beads were suspended in digestion buffer (Tris 50 mM pH 7.5, urea 2 M, 1 mM DTT and 5 µg.µl of
645 trypsin (Promega)) for 3 min at 30°C. Supernatants were transfer to new vials and beads were washed
646 twice using (Tris 50 mM pH 7.5, urea 2 M and iodoacetamide 5 mM). All washes were pulled and
647 incubated at 32°C for overnight digestion in the dark. Peptides were purified using C18 stage tips
648 protocol [79].
649
650 LC-MS/MS analysis of digested peptides was performed on an Orbitrap Q Exactive Plus mass
651 spectrometer (Thermo Fisher Scientific, Bremen) coupled to an EASY-nLC 1200 (Thermo Fisher
652 Scientific). A home-made column was used for peptide separation ($C_{18}$ 30 cm capillary column picotip
653 silica emitter tip (75 µm diameter filled with 1.9 µm Reprosil-Pur Basic $C_{18}$-HD resin, (Dr. Maisch GmbH,
654 Ammerbuch-Entringen, Germany)). It was equilibrated and peptide were loaded in solvent A (0.1 %
655 FA) at 900 bars. Peptides were separated at 250 $nl.min^{-1}$. Peptides were eluted using a gradient of
656 solvent B (80% ACN, 0.1 % FA) from 3% to 31% in 45 min, 31% to 60% in 17 min, 60% to 90% in 5 min
657 (total length of the chromatographic run was 82 min including high ACN level step and column
658 regeneration). Mass spectra were acquired in data-dependent acquisition mode with the XCalibur 2.2
659 software (Thermo Fisher Scientific, Bremen) with automatic switching between MS and MS/MS scans
660 using a top 12 method. MS spectra were acquired at a resolution of 70000 (at *m/z* 400) with a target
661 value of $3 \times 10^6$ ions. The scan range was limited from 300 to 1700 *m/z*. Peptide fragmentation was
662 performed using higher-energy collision dissociation (HCD) with the energy set at 27 NCE. Intensity
663 threshold for ions selection was set at $1 \times 10^6$ ions with charge exclusion of z = 1 and z > 7. The MS/MS
664 spectra were acquired at a resolution of 17500 (at *m/z* 400). Isolation window was set at 1.6 Th.
665 Dynamic exclusion was employed within 30 s. Recorded spectra were searched with MaxQuant
666 (version 1.5.3.8) using the Andromeda search engine[80] against a human database (74368 entries,
667 downloaded from Uniprot the 27th of September 2019), a Streptococcus pneumoniae R6 database
668 (2031 entries, downloaded from Uniprot the 1st of January 2020) and a Streptococcus pneumoniae
669 serotype 4 database (2115 entries, downloaded from Uniprot 1st of January 2020).
670
671 The following search parameters were applied: carbamidomethylation of cysteines was set as a fixed
672 modification, oxidation of methionine and protein N-terminal acetylation were set as variable
673 modifications. The mass tolerances in MS and MS/MS were set to 5 ppm and 20 ppm respectively.
674 Maximum peptide charge was set to 7 and 5 amino acids were required as minimum peptide length.
675 At least 2 peptides (including 1 unique peptides) were asked to report a protein identification. A false
676 discovery rate of 1% was set up for both protein and peptide levels. iBAQ value was calculated. The
677 match between runs features was allowed for biological replicate only.
678
679 For pull down of GFP-COMMD2, washed beads were re-suspended in 150 µl digestion buffer (20 mM
680 Tris.HCl pH 8.0, 2 mM $CaCl_2$) and incubated for 4 hours with 1 µg trypsin (Promega) at 37˚C and shaking
681 at 1200 rpm. Beads were removed, another 1 µg of trypsin was added and proteins were further
682 digested overnight at 37°C , shaking at 750 rpm. Peptides were acidified with trifluoroacetic acid (TFA)
683 to lower the pH below 3 and desalted on reversed phase (RP) C18 OMIX tips (Agilent). The tips were
684 first washed 3 times with 100 µl pre-wash buffer (0.1% TFA in water/acetonitrile (ACN, 20:80, v/v))
685 and pre-equilibrated 5 times with 100 µl of wash buffer (0.1% TFA in water) before the sample was
686 loaded on the tip. After peptide binding, the tip was washed 3 times with 100 µl of wash buffer and
687 peptides were eluted twice with 100 µl elution buffer (0.1% TFA in water/ACN (40:60, v/v)). The

688 combined elutions were transferred to HPLC inserts and dried in a vacuum concentrator. The peptides
689 were re-dissolved in 20 µl loading solvent A (0.1% TFA in water/ACN (98:2, v/v)) of which 2 µl was
690 injected for LC-MS/MS analysis on an Ultimate 3000 RSLCnano system in-line connected to a Q
691 Exactive HF mass spectrometer (Thermo). Trapping was performed at 10 µl/min for 4 min in loading
692 solvent A on a 20 mm trapping column (made in-house, 100 µm internal diameter (I.D.), 5 µm beads,
693 C18 Reprosil-HD, Dr. Maisch, Germany). The peptides were separated on an in-house produced
694 column (75 µm x 250 mm), equipped with a laser pulled electrospray tip using a P-2000 Laser Based
695 Micropipette Puller (Sutter Instruments), packed in-house with ReproSil-Pur basic 1.9 µm silica
696 particles (Dr. Maisch). The column was kept at a constant temperature of 50°C. Peptides eluted using
697 a non-linear gradient reaching 33% MS solvent B (0.1% FA in water/acetonitrile (2:8, v/v)) in 60 min,
698 55% MS solvent B in 75 min and 70% MS solvent B after 90 min at a constant flow rate of 300 nl/min.
699 This was followed by a 5-minutes wash at 70% MS solvent B and re-equilibration with MS solvent A
700 (0.1% FA in water). The mass spectrometer was operated in data-dependent mode, automatically
701 switching between MS and MS/MS acquisition for the 12 most abundant ion peaks per MS spectrum.
702 Full-scan MS spectra (375-1500 m/z) were acquired at a resolution of 60,000 in the Orbitrap analyzer
703 after accumulation to a target value of 3,000,000. The 12 most intense ions above a threshold value
704 of 13,000 were isolated (isolation window of 1.5 m/z) for fragmentation at a normalized collision
705 energy of 30% after filling the trap at a target value of 100,000 for maximum 80 ms. MS/MS spectra
706 (145-2,000 m/z) were acquired at a resolution of 15,000 in the Orbitrap analyzer. The
707 polydimethylcyclosiloxane background ion at 445.120028 Da was used for internal calibration (lock
708 mass) and QCloud [81] has been used to control instrument longitudinal performance during the project.
709 Recorded spectra were searched with MaxQuant (version 2.0.3.0) using the Andromeda search engine
710 with default search settings including a false discovery rate set at 1% on PSM, peptide and protein
711 level.
712
713 Spectra were searched against the *Streptococcus pneumonia setotype 4* (TIGR4) (Taxid: 170187)
714 protein sequences in the Uniprot database (database release version of 04_2022, UP000000585),
715 containing 2,109 sequences (www.uniprot.org), the *Streptococcus pneumoniae* (Taxid: 1313) protein
716 sequences in the Uniprot database (database release version of 04_2022, UP000046310), containing
717 2,115 sequences (www.uniprot.org) and the human protein sequences in the Swiss-Prot database
718 (database release version of 2022_01, reference proteome: UP000005640), containing 20,588
719 sequences (www.uniprot.org). The mass tolerance for precursor and fragment ions was set to 4.5 and
720 20 ppm, respectively, during the main search. Enzyme specificity was set as C-terminal to arginine and
721 lysine, also allowing cleavage at proline bonds with a maximum of three missed cleavages. Variable
722 modifications were set to oxidation of methionine residues, acetylation of protein N-termini and lysine
723 residues, phosphorylation of serine, threonine and tyrosine and ubiquitination of lysine residues.
724 Matching between runs was enabled with a matching time window of 0.7 minute and an alignment
725 time window of 20 minutes. Only proteins with at least one unique or razor peptide were retained
726 leading to the identification of 2,328 proteins. Proteins were quantified by the MaxLFQ algorithm
727 integrated in the MaxQuant software. A minimum ratio count of two unique or razor peptides was
728 required for quantification.
729
730 Data analysis for quantitative proteomics. Quantitative analysis was based on pairwise comparison of
731 protein intensities. Values were log-transformed (log2). Reverse hits and potential contaminant were
732 removed from the analysis. Proteins with at least 2 peptides were kept for further statistics after
733 removing shared proteins from the uninfected GFP alone control. Intensity values were normalized by
734 median centering within conditions (normalized function of the R package DAPAR [82]). Remaining
735 proteins without any iBAQ value in one of both conditions have been considered as proteins
736 quantitatively present in a condition and absent in the other. They have therefore been set aside and
737 considered as differentially abundant proteins. Next, missing values were imputed using the impute.
738 MLE function of the R package imp4p (https://rdrr.io/cran/imp4p/man/imp4p-package.html).

739 Statistical testing was conducted using a limma t-test thanks to the R package limma [83]. An adaptive
740 Benjamini-Hochberg procedure was applied on the resulting p-values thanks to the function adjust.p
741 of R package cp4p[84] using the robust method described in ([85]) to estimate the proportion of true null
742 hypotheses among the set of statistical tests. The proteins associated to an adjusted p-value inferior
743 to a FDR level of 1% have been considered as significantly differentially abundant proteins.
744
745 Statistical analysis. All experiments, unless otherwise noted, were biologically repeated 3–5 times and
746 the statistical test is reported in the figure legend. Data normality was tested by Shapiro-Wilk test, and
747 appropriate parametric or non-parametric tests performed depending on result. P values calculated
748 using GraphPad Prism software and the exact values are in source data. Microscopy data obtained
749 from analysis of 3 – 5 image fields per biological replicate after being automatically acquired by the
750 microscope software to ensure unbiased sampling with the total number of analyzed cells or nuclei
751 noted in the figure legend.
752
753 **Data Availability:**
754 All data in the present study is available upon request from the corresponding authors. The mass
755 spectrometry proteomics data of GFP-p65 and GFP-COMMD2 have been deposited to the
756 ProteomeXchange Consortium via the PRIDE partner repository with the dataset identifiers
757 PXD032970 (p65) and PXD043886 (COMMD2).
758
759 **Code Availability:**
760 No custom code or software was used in the manuscript.
761
762 **Acknowledgements:**
763 We would like to thank Emmanuelle Varon and Thomas Kohler for their generous gifts of *S. pneumonie*
764 strains. We are appreciative of Pierre-Henri Commere and the Institut Pasteur, Flow Cytometry
765 Platform (Paris, France) for sorting of the COMMD2 stable cell line. Finally, we like to thank Daniel
766 Hamaoui for his help processing blots during COVID-19 related work personnel restrictions. Michael
767 G. Connor is supported by a Springboard to Independence grant (AirwayStasis) from the French
768 Government's Investissement d'Avenir program, the Laboratoire d'Excellence ''Integrative Biology of
769 Emerging Infectious Diseases" (ANR-10-LABX-62-IBEID). Work in the laboratory Chromatin and
770 infection unit (headed by Melanie A. Hamon) is supported by the Institut Pasteur, the Fondation pour
771 la Recherche Médicale (FRM- EQU202003010152), the Fondation iXCore-iXLife and the Pasteur-
772 Weizmann research fund. Caroline M. Weight was supported by the Medical Research Council
773 (MR/T016329/1). Sebastian Baumgarten is supported by the Institut Pasteur and the European
774 Commission (ERC-STG "PlasmoEpiRNA"). The views expressed in this article are those of the authors
775 and not necessarily those of the NIHR, or the Department of Health and Social Care. Jost Enninga and
776 Lisa Sanchez, members of Dynamics of host-pathogen interactions unit (Institut Pasteur), are
777 supported by the European Commission (ERC-CoG-Endosubvert), the ANR-HBPsensing, and are
778 members of the IBEID and Milieu Interieur LabExes. Filipe Carvalho was supported by a postdoctoral
779 grant through the "Investissement d'Avenir" as part of a French "Laboratoire d'Excellence" (LabEx)
780 research program: Integrative Biology of Emerging Infectious Diseases (ANR-10-LBX-62 IBEID). This
781 work was also supported by EPIC-XS, project number 823839, funded by the Horizon 2020 program of
782 the European Union.
783
784
785 **Author contributions:**
786 Conceived and designed all experiments: MGC and MAH. Performed and analyzed data for all
787 experiments: MGC with specific contributions from LS (confocal microscopy imaging repeats); FC,
788 MGE, & TC (p65 mass spectrometry data, repeats for GFP & endogenous immunoprecipitations
789 validations, analysis…); CMW (Detroit562 immunoblot), FI, SD and SB (COMMD2 mass spectrometry

data, and analysis…), and CC (western blot and cell culture). MGC and MAH edited and reviewed the manuscript. MC and MAH supervised the research and secured funding. All authors approved the final manuscript.

**Conflict of interest statement:**

The authors declare no conflict of interest.

797 **Figure 1: TIGR4 antagonizes p65 activation in a pro-inflammatory environment but not NF-κB**
798 **nuclear translocation.** Immunoblot of A549 human airway epithelial cells 2 hrs post-challenge with
799 either IL-1β (10 ng/ml), TIGR4 (MOI 20) or 6B ST90 (MOI 20) (+/- IL-1β; 10 ng/ml). Whole cell lysates
800 probed for p65, phosphorylated p65 at Serine 276, phosphorylated p65 at Serine 536 or Actin. A)
801 Representative image of immunoblot. Actin normalized B) total p65, C) phosphorylated p65 at Serine
802 276 and D) phosphorylated p65 at Serine 536 (n=11 biological replicates). Dot blot with mean (red
803 line). One-way ANOVA with repeated measures with mixed-effects analysis comparing all means with
804 Tukey's multiple comparison post-hoc test. **P ≤ 0.01, ***P ≤ 0.001, ****P ≤ 0.0001. E)
805 Immunofluorescence confocal microscopy of paraformaldehyde fixed A549 cells 2 h post-challenge
806 with either IL-1β (10 ng/ml) or TIGR4 (+/- IL-1β 10 ng/ml; MOI 20) stained for p65 (cyan) and nucleus
807 (DAPI; gray). Scale bar = 100µm. F) Quantification of nuclear p65 normalized to the nuclei (n = 3
808 biological replicates with total nuclei counts for Uninfected n= 636, IL-1β n= 801, TIGR4 n=633, TIGR4
809 + IL-1β n=516). Tukey box and whisker plot with defined box boundaries being the upper and lower
810 interquartile range (IQR), 'whiskers' (fences) being ± 1.5 times IQR and the median depicted by the
811 middle solid line. Dots represent outliers. Two-way ANOVA comparing all means with Tukey's multiple
812 comparison post-hoc test. ****P ≤ 0.0001. Full blots provided in Supplementary Information 1.
813
814 **Figure 2: TIGR4 represses p65 dependent transcription in the presence of IL-1β even though p65 is**
815 **associated with chromatin.** A) Inflammatory gene transcription profiles by RT-qPCR for IL-6, IL-8,
816 PTGS2 & CSF2 of A549 cells over a 2 hr time course challenged with either IL-1β or TIGR4 (+/- IL-1β 10
817 ng/ml; MOI 20). Graphed as the relative expression of each indicated transcript to matched
818 uninfected/unstimulated control per time point (n = 3 biological replicates; 2 technicals per replicate).
819 Displayed as a dot plot with each data point and a bar representing the mean. 10µg chromatin input
820 from A549 cells either untreated (light gray), IL-1β treated (10 ng/ml; dark gray) or 2 hrs post-challenge
821 with TIGR4 (+/- IL-1β; 10 ng/ml; MOI 20; light blue or dark blue respectively). B) Schematic
822 representation of PTGS2 or CSF2 promoter with ChIP-qPCR primer locations and NF-κB sites denoted
823 as predicted by Alibaba2-curated eukaryotic transcription factor DNA-binding motifs from the
824 TRANSFAC database [67]. C & D) ChIP-qPCR represented as % recovery against input of p65 at indicated
825 NF-κB sites. Tukey box and whisker plot with defined box boundaries being the upper and lower
826 interquartile range (IQR), 'whiskers' (fences) being ± 1.5 times IQR and the median depicted by the
827 middle solid line (n=3 biological replicates with 2 or 3 technicals per replicate). One-way ANOVA
828 comparing all means with Tukey's multiple comparison post-hoc test. ns=not significant, ****P ≤
829 0.0001.
830
831 **Figure 3: TIGR4 induces a divergent p65 interactome leading to NF-kB p65 turnover by aggrephagy.**
832 Mass-spectrometry interactome (n=4 biological replicates per condition) of immunoprecipitated GFP-
833 p65 from a stable A549 GFP-p65 cell line ($1x10^7$ cells total) 2 hrs post challenge with either 6B ST90
834 (MOI 20) or TIGR4 (MOI 20). A) Volcano plot of identified interacting partners with known NF-kB p65
835 partners in blue and general significant targets in yellow. Lines represent -log10(pV) and fold-change
836 (log2) cutoffs with targets of interested denoted. B) Representative immunoblot of A549 whole cell
837 lysates 2 hrs post-challenge with either IL-1β (10 ng/ml), TIGR4 (MOI 20) or 6B ST90 (MOI 20) (+/- IL-
838 1β; 10 ng/ml) probed for RelB, HDAC6, or Actin. C & D) Quantification of RelB or HDAC6 levels
839 normalized to Actin (n=4 biological replicates). Displayed as a dot blot with mean (red line). One-way
840 ANOVA with repeated measures with mixed-effects analysis comparing all means. *P ≤ 0.05, **P ≤
841 0.01, ***P ≤ 0.001. Whole cell lysates from A549 cells 2 hrs post-challenge with either IL-1β (10 ng/ml)
842 or TIGR4 (MOI 20; +/- IL-1β; 10 ng/ml) from E) Bafilomycin A1 (400nM) or G) SAR405 (500nM)
843 pretreated cells (both 3 hrs) and immunoblots probed for p65 or actin (n=3 biological replicates).
844 Quantified levels of total p65 normalized to actin from F) Bafilomycin A1 (400nM) or H) SAR405

845 (500nM). Dot blot with mean (red line). One-way ANOVA with repeated measures with mixed-effects
846 analysis comparing all means. ns = not significant. Full blots provided in Supplementary Information 2
847
848 **Figure 4: TIGR4 drives NF-kB p65 interaction with COMMD2 and p62 (SQSTM1) and nuclear**
849 **translocation.** Immunoprecipitates using GFP-Trap agarose beads were collected from a stable A549
850 GFP-COMMD2 cell line 2 hrs post-challenge with either IL-1β (10 ng/ml) or TIGR4 (MOI 20; +/- IL-1β;
851 10 ng/ml). A) A single representative immunoblot from 3 biological replicates of GFP-COMMD2
852 immunoprecipitation lysates (input & IP) probed for p65 or GFP.. B) Representative immunoblot from
853 3 biological replicates of GFP-COMMD2 immunoprecipitation lysates (input & IP) probed for p62 or
854 GFP. Full blots provided in Supplementary Information 3. C) Immunofluorescence confocal microscopy
855 of stable A549 GFP-COMMD2 cells 2 h post-challenge with either IL-1β (10 ng/ml) or TIGR4 (+/- IL-1β
856 10 ng/ml; MOI 20) stained for p62 (magenta) against GFP-COMMD2 (gray). Scale bar = 100 µm. Red
857 inset images of single cell highlighting (white arrow) perinuclear punta. Inset scale bar 10 µm.
858 Quantification of total cellular p62 D) normalized to cell area (GFP-COMMD2 signal) and nuclear p62
859 E) normalized to the area of the nucleus (DAPI signal; n = 3 biological replicates with total cell counts
860 for Uninfected n= 548, IL-1β n= 670, TIGR4 n=356, TIGR4 + IL-1β n=271). Quantification of total cellular
861 COMMD2 F) normalized to cell area (GFP-COMMD2 signal) and nuclear COMMD2 G) normalized to
862 the area of the nucleus (DAP I signal; n = 3 biological replicates with total cell counts for Uninfected
863 n= 864, IL-1β n= 1068, TIGR4 n=596, TIGR4 + IL-1β n=534). Tukey box and whisker plot with defined
864 box boundaries being the upper and lower interquartile range (IQR), 'whiskers' (fences) being ± 1.5
865 times IQR and the median depicted by the middle solid line. Dots represent outliers. Two-way ANOVA
866 comparing all means with Tukey's multiple comparison post-hoc test. **P ≤ 0.01, ***P ≤ 0.001, ****P
867 ≤ 0.0001. H) Cell fractions from a stable A549 GFP-COMMD2 cell line 2 hrs post-challenge with either
868 IL-1β (10 ng/ml) or TIGR4 (MOI 20; +/- IL-1β; 10 ng/ml). Representative immunoblot probed for GFP
869 (COMMD2) enrichment across cellular compartments. GapDH or histone H4 (H4) used to determine
870 fraction purity. Full blots provided in Supplementary Information 3. I) Percent nuclear COMMD2 levels
871 normalized to input (n=3 biological replicates). Graphed as mean ± STD with dots representing
872 individual biological replicates. One-way ANOVA with repeated measures with mixed-effects analysis
873 comparing all means with Tukey's multiple comparison post-hoc test. ****P ≤ 0.0001.
874
875 **Figure 5: COMMD2-p65-p62 is exported from nucleus through CRM1.** Immunofluorescence confocal
876 microscopy of stable A549 GFP-COMMD2 pretreated for 3 hrs with Leptomycin B (10 nM) prior to 2
877 hr challenge with either IL-1β (10 ng/ml) or TIGR4 (MOI 20). Paraformaldehyde fixed cells stained for
878 A) p62 (magenta), or B) p65 (cyan) against GFP-COMMD2 (gray) and nuclei (DAPI; blue). Scale bar =
879 100 µm or 10 µm for uninfected and untreated single cell inserts. Nuclear levels of C) GFP-COMMD2
880 or D) p62 normalized to the segmented nuclei using DAPI signal (n = 3 biological replicates with total
881 nuclei counts for Uninfected (-) n=1664, Uninfected n= 742, IL-1β (-) n=1068, IL-1β n= 920, TIGR4 (-)
882 n=585, TIGR4 n=798). E) Nuclear levels of p65 normalized to the segmented nuclei using DAPI signal
883 (n = 3 biological replicates with total nuclei counts for Uninfected (-) n=489, Uninfected n= 1492, IL-1β
884 (-) n=576 IL-1β n= 1658, TIGR4 (-) n=680, TIGR4 n=1514). Tukey box and whisker plot with defined box
885 boundaries being the upper and lower interquartile range (IQR), 'whiskers' (fences) being ± 1.5 times
886 IQR and the median depicted by the middle solid line. Dots represent outliers. Two-way ANOVA
887 comparing all means with Tukey's multiple comparison post-hoc test. ***P ≤ 0.001, ****P ≤ 0.0001.
888 F) Representative immunofluorescence confocal microscopy of stable A549 GFP-COMMD2 pretreated
889 for 3 hrs with Leptomycin B (10nM) prior to 2 hr challenge TIGR4 (MOI 20; +/- IL-1β; 10 ng/ml).
890 Paraformaldehyde fixed cells stained for p62 (magenta) against GFP-COMMD2 (gray) and nuclei (DAPI;
891 blue). Scale bar = 10µm G) Nuclear p62 puncta quantification (n = 3 biological replicates with total
892 nuclei counts for Uninfected n=1041, IL-1β n=831, TIGR4 n=1164, TIGR4 + IL-1β n=1269). Graphed as

893 mean with dots representing individual biological replicates. One-way ANOVA comparing all means
894 with Tukey's multiple comparison post-hoc test. *P ≤ 0.05, **P ≤ 0.01, ****P ≤ 0.0001.
895
896 **Figure 6: COMMD2 nuclear localization is dependent on pneumolysin.** A) Immunofluorescence
897 deconvolution epifluorescence microscopy of paraformaldehyde fixed stable A549 GFP-COMMD2
898 cells 2 h post-challenge with either IL-1β (10 ng/ml), TIGR4 wildtype (MOI 20), TIGR4 *Δply* (MOI 20), or
899 TIGR4 *ΔspxB* (MOI 20) with GFP-COMMD2 (gray). Scale bar = 10µm. B) Quantification of nuclear GFP-
900 COMMD2 normalized to the segmented nuclei using DAPI signal (omitted in representative images for
901 phenotype clarity; n = 3 biological replicates with total nuclei counts for Uninfected n= 6292, IL-1β n=
902 6579, TIGR4 n=5061, TIGR4 ΔPly n=7607, TIGR4 ΔSpxB n=6566). Graphed as mean ± STD with dots
903 representing individual biological replicates. One-way ANOVA comparing all means with Tukey's
904 multiple comparison post-hoc test. *P ≤ 0.05, **P ≤ 0.01. C) Immunofluorescence deconvolution
905 epifluorescence microscopy of paraformaldehyde fixed stable A549 GFP-COMMD2 cells 2 hr post-
906 challenge with either indicated pneumococcus strains at MOI 20. Scale bar = 10µm. D) Quantification
907 of nuclear GFP-COMMD2 normalized to the segmented nuclei using DAPI signal (omitted in
908 representative images for phenotype clarity; n = 3 biological replicates with total nuclei counts for
909 Uninfected n= 469, 6B ST90 n=666, 6B ST138 n=566, TIGR4 n=571, JW TIGR4 WT (parent to JW TIGR4
910 ΔCPS) n=553, JW TIGR4 ΔCPS n=700 and Graphed as mean ± STD with dots representing individual
911 biological replicates. Two-way ANOVA comparing means with Tukey's multiple comparison post-hoc
912 test. ns = not significant, ****P ≤ 0.0001.
913
914 **Figure 7: TIGR4 drives distinct COMMD2 interacting partners with enzymatic activity and associated**
915 **with RNA transcription.** Mass-spectrometry interactome (n=2 biological replicates per condition) of
916 immunoprecipitated GFP-COMMD2 from a stable A549 GFP-COMMD2 cell line ($1x10^7$ cells total) 2 hrs
917 post challenge with either A) TIGR4 (MOI 20), B) 6B ST90 (MOI 20) or C) IL-1β (10 ng/ml) . Shown as
918 volcano plot to uninfected control with identified interacting partners with known NF-kB p65
919 interaction in blue and significant targets in yellow. Lines represent -log10(pV) and fold-change cutoffs
920 with targets of interested denoted. D) Venn diagram describing the numbers of unique and shared
921 significant proteins and their total % from the mass-spectrometry dataset. Table break down of
922 identified partners that were significant, of the significant targets that are unique, and of the
923 significant targets shared with the p65 interactome. E) Panther classification analysis of protein class
924 of identified COMMD2 interactors unique to TIGR4, shared between TIGR4 and 6B ST90, or unique to
925 6B ST90.
926
927 **Figure 8: COMMD2 RNAi increases cytokine production.** A) Representative whole cell lysate
928 immunoblot of 72 hr RNAi targeting COMMD2 or p62 in primary human nasal epithelial cells. PVDF
929 membrane probed for either COMMD2 or p62 protein levels after 2 hr challenge with either IL-1β (10
930 ng/ml) or TIGR4 (MOI 20) +/- IL-1β (10 ng/ml). B & C) quantification of COMMD2 and p62 protein
931 levels post RNAi. Dot blot with mean (bars) ± STD. One-way ANOVA comparing all means by Fisher's
932 LSD test. ****P ≤ 0.0001. D & E) Cytokine levels from primary human nasal epithelial cells (n = 4
933 biological replicates with 2 technicals per replicate) after 72 hr RNAi targeting COMMD2 or p62 and
934 followed by challenge for 2 hrs with either IL-1β (10 ng/ml) or TIGR4 (MOI 20) +/- IL-1β (10 ng/ml). Dot
935 blot with mean (bars) ± STD. One-way ANOVA comparing all means by Fisher's LSD test. ns = not
936 significant, *P ≤ 0.05, **P ≤ 0.01, ****P ≤ 0.0001. Full blots provided in Supplementary Information 4.
937
938 **Sup. Figure 1: TIGR4 dampens p65 activation over time.** A) Representative graph of actin normalized
939 phosphorylated p65 S536 levels over 2 hrs quantified by immunoblot. B) Immunoblot of whole cell
940 lysates obtained from primary human nasal epithelial cells 2 hrs post-challenge with either IL-1β (10

941 ng/ml), TIGR4 (MOI 20) or 6B ST90 (MOI 20) (+/- IL-1β; 10 ng/ml). PVDF membrane probed for
942 phosphorylated p65 Serine 536 or Actin (n=2 biological replicates). C) Immunoblot of whole cell
943 Detroit 562 cell lysates 2 hrs post-challenge with either TIGR4 (MOI 10) or 6B ST90 (MOI 10).
944 Nitrocellulose membrane probed for phosphorylated p65 Serine 536 or GapDH (n=2 biological
945 replicates).
946
947 **Sup. Figure 2: Proteasomal degradation is not involved in TIGR4 mediated p65 turnover.** A)
948 Quantification and representative immunoblot image of MG132 (10µM; 3 hr pretreatment) treated
949 A549 whole cell lysates 2 hrs post-challenge with either IL-1β (10 ng/ml), TIGR4 (MOI 20) or 6B ST90
950 (MOI 20) (+/- IL-1β; 10 ng/ml) and probed for total p65 or actin (n=11 biological replicates). Dot blot
951 with mean (red line). One-way ANOVA with repeated measures with mixed-effects analysis comparing
952 all means with Tukey's multiple comparison post-hoc test. ns=not significant, ****P ≤ 0.0001. B)
953 Representative immunoblot of whole cell lysates collected from primary human nasal epithelial cells
954 treated with Bafilomycin A1 (400nM; 3 hrs) prior to 2 hr challenge with either IL-1β (10 ng/ml) or
955 TIGR4 (MOI 20; +/- IL-1β; 10 ng/ml). PVDF membrane probed for levels of p65 and actin. C)
956 Representative immunoblot of endogenous p65 immunoprecipitation (input & IP) from $1x10^7$ A549
957 cells post 2 hr challenge using protein G sepharose beads. Collected lysates probed for p65, RelB or
958 NFkB1 (p105/p50).
959
960 **Sup. Figure 3: TIGR4 specifically drives COMMD2 translocation and inhibiting aggrephagy increases**
961 **total complex components.** A) Cell fractions from a stable A549 GFP-COMMD2 cell line 2 hrs post-
962 challenge with either IL-1β (10 ng/ml), TIGR4 (MOI 20) or 6B ST90 (MOI 20). Representative
963 immunoblot of cell fractions and coomassie stained PVDF membranes. Blots probed for GFP
964 (COMMD2) enrichment across cellular compartments. Quantified immunofluorescence confocal
965 microscopy of A549 GFP-COMMD2 cells pretreated with Bafilomycin A1 (400nM; 3 hrs) prior to 2 hr
966 challenge with either IL-1β (10 ng/ml) or TIGR4 (MOI 20; +/- IL-1β; 10 ng/ml). Paraformaldehyde fixed
967 and stained for B) p65, C) COMMD2 or D) p62. (n = 3 biological replicates with total cell count for
968 Uninfected p62 & COMMD2 n=1648 & p65 n=1496, IL-1β p62 & COMMD2 n=2103 & p65 n=1703,
969 TIGR4 p62 & COMMD2 n=2033 & p65 n=1597, TIGR4 + IL-1β p62 & COMMD2 n=1724 & p65 n=1759).
970 Tukey box and whisker plot with defined box boundaries being the upper and lower interquartile
971 range (IQR), 'whiskers' (fences) being ± 1.5 times IQR and the median depicted by the middle solid
972 line. Dots represent outliers. Two-way ANOVA comparing all means with Tukey's multiple comparison
973 post-hoc test. ns=not significant, ***P ≤ 0.001,****P ≤ 0.0001.
974
975

976 **References**


977 1 Ghosh, S. & Hayden, M. S. New regulators of NF-kappaB in inflammation. *Nature reviews.*
978 *Immunology* **8**, 837-848, doi:10.1038/nri2423 (2008).
979 2 Bhatt, D. & Ghosh, S. Regulation of the NF-kappaB-Mediated Transcription of Inflammatory
980 Genes. *Frontiers in immunology* **5**, 71, doi:10.3389/fimmu.2014.00071 (2014).
981 3 Rahman, M. M. & McFadden, G. Modulation of NF-κB signalling by microbial pathogens.
982 *Nature Reviews Microbiology* **9**, 291-306, doi:10.1038/nrmicro2539 (2011).
983 4 Brücher, B., Lang, F. & Jamall, I. NF-kB signaling and crosstalk during carcinogenesis. *4open* **2**,
984 1-35, doi:10.1051/fopen/2019010 (2019).
985 5 Hoffmann, A., Natoli, G. & Ghosh, G. Transcriptional regulation via the NF-κB signaling module.
986 *Oncogene* **25**, 6706-6716, doi:10.1038/sj.onc.1209933 (2006).
987 6 Basak, S. & Hoffmann, A. Crosstalk via the NF-kappaB signaling system. *Cytokine & growth*
988 *factor reviews* **19**, 187-197, doi:10.1016/j.cytogfr.2008.04.005 (2008).
989 7 Shih, V. F.-S., Tsui, R., Caldwell, A. & Hoffmann, A. A single NFκB system for both canonical and
990 non-canonical signaling. *Cell research* **21**, 86-102, doi:10.1038/cr.2010.161 (2011).
991 8 Huxford, T. & Ghosh, G. A structural guide to proteins of the NF-kappaB signaling module. *Cold*
992 *Spring Harbor perspectives in biology* **1**, a000075, doi:10.1101/cshperspect.a000075 (2009).
993 9 Wong, D. *et al.* Extensive characterization of NF-κB binding uncovers non-canonical motifs and
994 advances the interpretation of genetic functional traits. *Genome biology* **12**, R70-R70,
995 doi:10.1186/gb-2011-12-7-r70 (2011).
996 10 Christian, F., Smith, E. L. & Carmody, R. J. The Regulation of NF-κB Subunits by
997 Phosphorylation. *Cells* **5**, 12, doi:10.3390/cells5010012 (2016).
998 11 Oeckinghaus, A. & Ghosh, S. The NF-κB Family of Transcription Factors and Its Regulation. *Cold*
999 *Spring Harbor perspectives in biology* **1**, a000034, doi:10.1101/cshperspect.a000034 (2009).
1000 12 Bartuzi, P., Hofker, M. H. & van de Sluis, B. Tuning NF-κB activity: A touch of COMMD proteins.
1001 *Biochimica et Biophysica Acta (BBA) - Molecular Basis of Disease* **1832**, 2315-2321,
1002 doi:https://doi.org/10.1016/j.bbadis.2013.09.014 (2013).
1003 13 Newton, K. & Dixit, V. M. Signaling in innate immunity and inflammation. *Cold Spring Harbor*
1004 *perspectives in biology* **4**, doi:10.1101/cshperspect.a006049 (2012).
1005 14 Burstein, E. *et al.* COMMD proteins, a novel family of structural and functional homologs of
1006 MURR1. *The Journal of biological chemistry* **280**, 22222-22232, doi:10.1074/jbc.M501928200
1007 (2005).
1008 15 de Bie, P. *et al.* Characterization of COMMD protein-protein interactions in NF-kappaB
1009 signalling. *The Biochemical journal* **398**, 63-71, doi:10.1042/BJ20051664 (2006).
1010 16 Maine, G. N., Mao, X., Komarck, C. M. & Burstein, E. COMMD1 promotes the ubiquitination of
1011 NF-kappaB subunits through a cullin-containing ubiquitin ligase. *Embo J* **26**, 436-447,
1012 doi:10.1038/sj.emboj.7601489 (2007).
1013 17 Maine, G. N. & Burstein, E. COMMD proteins and the control of the NF kappa B pathway. *Cell*
1014 *Cycle* **6**, 672-676, doi:10.4161/cc.6.6.3989 (2007).
1015 18 Maine, G. N. & Burstein, E. COMMD proteins: COMMing to the scene. *Cellular and molecular*
1016 *life sciences : CMLS* **64**, 1997-2005, doi:10.1007/s00018-007-7078-y (2007).
1017 19 Riera-Romo, M. COMMD1: A Multifunctional Regulatory Protein. *Journal of cellular*
1018 *biochemistry* **119**, 34-51, doi:10.1002/jcb.26151 (2018).
1019 20 Geng, H., Wittwer, T., Dittrich-Breiholz, O., Kracht, M. & Schmitz, M. L. Phosphorylation of NF-
1020 kappaB p65 at Ser468 controls its COMMD1-dependent ubiquitination and target gene-
1021 specific proteasomal elimination. *EMBO Rep* **10**, 381-386, doi:10.1038/embor.2009.10 (2009).
1022 21 Thoms, H. C. *et al.* Nucleolar Targeting of RelA(p65) Is Regulated by COMMD1-Dependent
1023 Ubiquitination. *Cancer research* **70**, 139-149, doi:10.1158/0008-5472.Can-09-1397 (2010).
1024 22 Mao, X. *et al.* COMMD1 (copper metabolism MURR1 domain-containing protein 1) regulates
1025 Cullin RING ligases by preventing CAND1 (Cullin-associated Nedd8-dissociated protein 1)

1026 binding. *The Journal of biological chemistry* **286**, 32355-32365, doi:10.1074/jbc.M111.278408
1027 (2011).
1028 23 Johannessen, M., Askarian, F., Sangvik, M. & Sollid, J. E. Bacterial interference with canonical
1029 NFκB signalling. *Microbiology (Reading, England)* **159**, 2001-2013, doi:10.1099/mic.0.069369-
1030 0 (2013).
1031 24 Connor, M. G. *et al.* The histone demethylase KDM6B fine-tunes the host response to
1032 Streptococcus pneumoniae. *Nature Microbiology*, doi:10.1038/s41564-020-00805-8 (2020).
1033 25 Quinton, L. J. *et al.* Functions and regulation of NF-kappaB RelA during pneumococcal
1034 pneumonia. *Journal of immunology (Baltimore, Md. : 1950)* **178**, 1896-1903,
1035 doi:10.4049/jimmunol.178.3.1896 (2007).
1036 26 Ferreira, D. M. *et al.* Controlled human infection and rechallenge with Streptococcus
1037 pneumoniae reveals the protective efficacy of carriage in healthy adults. *American journal of*
1038 *respiratory and critical care medicine* **187**, 855-864, doi:10.1164/rccm.201212-2277OC
1039 (2013).
1040 27 Henriques-Normark, B. & Tuomanen, E. I. The Pneumococcus: Epidemiology, Microbiology,
1041 and Pathogenesis. *Cold Spring Harbor perspectives in medicine* **3**, a010215,
1042 doi:10.1101/cshperspect.a010215 (2013).
1043 28 Jochems, S. P., Weiser, J. N., Malley, R. & Ferreira, D. M. The immunological mechanisms that
1044 control pneumococcal carriage. *PLoS pathogens* **13**, e1006665-e1006665,
1045 doi:10.1371/journal.ppat.1006665 (2017).
1046 29 Robson, R. L., Reed, N. A. & Horvat, R. T. Differential activation of inflammatory pathways in
1047 A549 type II pneumocytes by Streptococcus pneumoniae strains with different adherence
1048 properties. *BMC infectious diseases* **6**, 71, doi:10.1186/1471-2334-6-71 (2006).
1049 30 Weight, C. M. *et al.* Microinvasion by Streptococcus pneumoniae induces epithelial innate
1050 immunity during colonisation at the human mucosal surface. *Nature communications* **10**,
1051 3060, doi:10.1038/s41467-019-11005-2 (2019).
1052 31 Dong, W. *et al.* Streptococcus pneumoniae Infection Promotes Histone H3 Dephosphorylation
1053 by Modulating Host PP1 Phosphatase. *Cell reports* **30**, 4016-4026.e4014,
1054 doi:https://doi.org/10.1016/j.celrep.2020.02.116 (2020).
1055 32 Connor, M. G. *et al.* The histone demethylase KDM6B fine-tunes the host response to
1056 Streptococcus pneumoniae. *Nat Microbiol* **6**, 257-269, doi:10.1038/s41564-020-00805-8
1057 (2021).
1058 33 Kim, S. *et al.* Stress-induced NEDDylation promotes cytosolic protein aggregation through
1059 HDAC6 in a p62-dependent manner. *iScience* **24**, 102146,
1060 doi:https://doi.org/10.1016/j.isci.2021.102146 (2021).
1061 34 Lamark, T. & Johansen, T. Aggrephagy: Selective Disposal of Protein Aggregates by
1062 Macroautophagy. *International Journal of Cell Biology* **2012**, 736905,
1063 doi:10.1155/2012/736905 (2012).
1064 35 Svenning, S. & Johansen, T. Selective autophagy. *Essays in biochemistry* **55**, 79-92,
1065 doi:10.1042/bse0550079 (2013).
1066 36 Lee, D. H. & Goldberg, A. L. Proteasome inhibitors: valuable new tools for cell biologists.
1067 *Trends in cell biology* **8**, 397-403, doi:10.1016/s0962-8924(98)01346-4 (1998).
1068 37 Mauvezin, C. & Neufeld, T. P. Bafilomycin A1 disrupts autophagic flux by inhibiting both V-
1069 ATPase-dependent acidification and Ca-P60A/SERCA-dependent autophagosome-lysosome
1070 fusion. *Autophagy* **11**, 1437-1438, doi:10.1080/15548627.2015.1066957 (2015).
1071 38 Dröse, S. & Altendorf, K. Bafilomycins and concanamycins as inhibitors of V-ATPases and P-
1072 ATPases. *J Exp Biol* **200**, 1-8, doi:10.1242/jeb.200.1.1 (1997).
1073 39 Pasquier, B. Autophagy inhibitors. *Cellular and molecular life sciences : CMLS* **73**, 985-1001,
1074 doi:10.1007/s00018-015-2104-y (2016).
1075 40 Pasquier, B. SAR405, a PIK3C3/VPS34 inhibitor that prevents autophagy and synergizes with
1076 MTOR inhibition in tumor cells. *Autophagy* **11**, doi:10.1080/15548627.2015.1033601 (2015).

41 Vonk, W. I. M. *et al.* The Copper Metabolism MURR1 Domain Protein 1 (COMMD1) Modulates the Aggregation of Misfolded Protein Species in a Client-Specific Manner. *PloS one* **9**, e92408, doi:10.1371/journal.pone.0092408 (2014).

42 Tan, S. & Wong, E. in *Methods in Enzymology* Vol. 588 (eds Lorenzo Galluzzi, José Manuel Bravo-San Pedro, & Guido Kroemer) 245-281 (Academic Press, 2017).

43 Johansen, T. & Lamark, T. Selective autophagy mediated by autophagic adapter proteins. *Autophagy* **7**, 279-296 (2011).

44 Johnston, J. A., Ward, C. L. & Kopito, R. R. Aggresomes: a cellular response to misfolded proteins. *The Journal of cell biology* **143**, 1883-1898 (1998).

45 Lobb, I. T. *et al.* A Role for the Autophagic Receptor, SQSTM1/p62, in Trafficking NF-κB/RelA to Nucleolar Aggresomes. *Molecular Cancer Research* **19**, 274, doi:10.1158/1541-7786.MCR-20-0336 (2021).

46 Ryu, H. W., Won, H. R., Lee, D. H. & Kwon, S. H. HDAC6 regulates sensitivity to cell death in response to stress and post-stress recovery. *Cell stress & chaperones* **22**, 253-261, doi:10.1007/s12192-017-0763-3 (2017).

47 Wong, E. *et al.* Molecular determinants of selective clearance of protein inclusions by autophagy. *Nature communications* **3**, 1240, doi:10.1038/ncomms2244 (2012).

48 Kudo, N. *et al.* Leptomycin B inactivates CRM1/exportin 1 by covalent modification at a cysteine residue in the central conserved region. *Proceedings of the National Academy of Sciences of the United States of America* **96**, 9112-9117, doi:10.1073/pnas.96.16.9112 (1999).

49 Weiser, J. N., Ferreira, D. M. & Paton, J. C. Streptococcus pneumoniae: transmission, colonization and invasion. *Nature reviews. Microbiology* **16**, 355-367, doi:10.1038/s41579-018-0001-8 (2018).

50 Kadioglu, A., Weiser, J. N., Paton, J. C. & Andrew, P. W. The role of Streptococcus pneumoniae virulence factors in host respiratory colonization and disease. *Nature reviews. Microbiology* **6**, 288-301, doi:10.1038/nrmicro1871 (2008).

51 Bryant, J. C. *et al.* Pyruvate oxidase of Streptococcus pneumoniae contributes to pneumolysin release. *BMC microbiology* **16**, 271, doi:10.1186/s12866-016-0881-6 (2016).

52 Singla, A. *et al.* Endosomal PI(3)P regulation by the COMMD/CCDC22/CCDC93 (CCC) complex controls membrane protein recycling. *Nature communications* **10**, 4271, doi:10.1038/s41467-019-12221-6 (2019).

53 You, G. *et al.* COMMD proteins function and their regulating roles in tumors. *Frontiers in oncology* **13**, doi:10.3389/fonc.2023.1067234 (2023).

54 Das, T., Chen, Z., Hendriks, R. W. & Kool, M. A20/Tumor Necrosis Factor α-Induced Protein 3 in Immune Cells Controls Development of Autoinflammation and Autoimmunity: Lessons from Mouse Models. *Frontiers in immunology* **9**, doi:10.3389/fimmu.2018.00104 (2018).

55 Moreno, R., Sobotzik, J.-M., Schultz, C. & Schmitz, M. L. Specification of the NF-κB transcriptional response by p65 phosphorylation and TNF-induced nuclear translocation of IKKε. *Nucleic acids research* **38**, 6029-6044, doi:10.1093/nar/gkq439 (2010).

56 Collins, P. E., Mitxitorena, I. & Carmody, R. J. The Ubiquitination of NF-κB Subunits in the Control of Transcription. *Cells* **5**, 23, doi:10.3390/cells5020023 (2016).

57 Lanucara, F. *et al.* Dynamic phosphorylation of RelA on Ser42 and Ser45 in response to TNFalpha stimulation regulates DNA binding and transcription. *Open Biol* **6**, doi:10.1098/rsob.160055 (2016).

58 Saccani, S., Pantano, S. & Natoli, G. p38-Dependent marking of inflammatory genes for increased NF-kappa B recruitment. *Nature immunology* **3**, 69-75, doi:10.1038/ni748 (2002).

59 Quinton, L. J. & Mizgerd, J. P. Dynamics of lung defense in pneumonia: resistance, resilience, and remodeling. *Annual review of physiology* **77**, 407-430, doi:10.1146/annurev-physiol-021014-071937 (2015).

60 Pechous, R. D. With Friends Like These: The Complex Role of Neutrophils in the Progression of Severe Pneumonia. *Frontiers in cellular and infection microbiology* **7**, 160-160, doi:10.3389/fcimb.2017.00160 (2017).
61 Liu, J. *et al.* Advanced Role of Neutrophils in Common Respiratory Diseases. *Journal of immunology research* **2017**, 6710278, doi:10.1155/2017/6710278 (2017).
62 Craig, A., Mai, J., Cai, S. & Jeyaseelan, S. Neutrophil Recruitment to the Lungs during Bacterial Pneumonia. *Infection and immunity* **77**, 568-575, doi:10.1128/IAI.00832-08 (2009).
63 Pechous, R. D., Sivaraman, V., Stasulli, N. M. & Goldman, W. E. Pneumonic Plague: The Darker Side of Yersinia pestis. *Trends in microbiology*, doi:10.1016/j.tim.2015.11.008 (2015).
64 Yamamoto, K. *et al.* Roles of lung epithelium in neutrophil recruitment during pneumococcal pneumonia. *American journal of respiratory cell and molecular biology* **50**, 253-262, doi:10.1165/rcmb.2013-0114OC (2014).
65 Bou Ghanem, E. N. *et al.* Extracellular Adenosine Protects against Streptococcus pneumoniae Lung Infection by Regulating Pulmonary Neutrophil Recruitment. *PLoS pathogens* **11**, e1005126, doi:10.1371/journal.ppat.1005126 (2015).
66 Livak, K. J. & Schmittgen, T. D. Analysis of relative gene expression data using real-time quantitative PCR and the 2(-Delta Delta C(T)) Method. *Methods (San Diego, Calif.)* **25**, 402-408, doi:10.1006/meth.2001.1262 (2001).
67 Nguyen, L. K., Cavadas, M. A. S., Kholodenko, B. N., Frank, T. D. & Cheong, A. Species differential regulation of COX2 can be described by an NFκB-dependent logic AND gate. *Cellular and molecular life sciences : CMLS* **72**, 2431-2443, doi:10.1007/s00018-015-1850-1 (2015).
68 Huang, F., Spangler, J. R. & Huang, A. Y. In vivo cloning of up to 16 kb plasmids in E. coli is as simple as PCR. *PloS one* **12**, e0183974, doi:10.1371/journal.pone.0183974 (2017).
69 Watson, J. F. & García-Nafría, J. In vivo DNA assembly using common laboratory bacteria: A re-emerging tool to simplify molecular cloning. *The Journal of biological chemistry* **294**, 15271-15281, doi:10.1074/jbc.REV119.009109 (2019).
70 Thuring, R. W., Sanders, J. P. & Borst, P. A freeze-squeeze method for recovering long DNA from agarose gels. *Analytical biochemistry* **66**, 213-220, doi:10.1016/0003-2697(75)90739-3 (1975).
71 Tautz, D. & Renz, M. An optimized freeze-squeeze method for the recovery of DNA fragments from agarose gels. *Analytical biochemistry* **132**, 14-19, doi:10.1016/0003-2697(83)90419-0 (1983).
72 Jin, Z. *et al.* The hyperactive Sleeping Beauty transposase SB100X improves the genetic modification of T cells to express a chimeric antigen receptor. *Gene therapy* **18**, 849-856, doi:10.1038/gt.2011.40 (2011).
73 Kowarz, E., Loscher, D. & Marschalek, R. Optimized Sleeping Beauty transposons rapidly generate stable transgenic cell lines. *Biotechnology journal* **10**, 647-653, doi:10.1002/biot.201400821 (2015).
74 Laemmli, U. K. Cleavage of Structural Proteins during the Assembly of the Head of Bacteriophage T4. *Nature* **227**, 680-685, doi:10.1038/227680a0 (1970).
75 Schindelin, J. *et al.* Fiji: an open-source platform for biological-image analysis. *Nature methods* **9**, 676-682, doi:10.1038/nmeth.2019 (2012).
76 Kamentsky, L. *et al.* Improved structure, function and compatibility for CellProfiler: modular high-throughput image analysis software. *Bioinformatics (Oxford, England)* **27**, 1179-1180, doi:10.1093/bioinformatics/btr095 (2011).
77 McQuin, C. *et al.* CellProfiler 3.0: Next-generation image processing for biology. *PLoS biology* **16**, e2005970, doi:10.1371/journal.pbio.2005970 (2018).
78 Stirling, D. R., Carpenter, A. E. & Cimini, B. A. CellProfiler Analyst 3.0: accessible data exploration and machine learning for image analysis. *Bioinformatics (Oxford, England)* **37**, 3992-3994, doi:10.1093/bioinformatics/btab634 (2021).

1177 79 Kulak, N. A., Pichler, G., Paron, I., Nagaraj, N. & Mann, M. Minimal, encapsulated proteomic-
1178 sample processing applied to copy-number estimation in eukaryotic cells. *Nature methods* **11**,
1179 319-324, doi:10.1038/nmeth.2834 (2014).
1180 80 Tyanova, S., Temu, T. & Cox, J. The MaxQuant computational platform for mass spectrometry-
1181 based shotgun proteomics. *Nature protocols* **11**, 2301-2319, doi:10.1038/nprot.2016.136
1182 (2016).
1183 81 Olivella, R. *et al.* QCloud2: An Improved Cloud-based Quality-Control System for Mass-
1184 Spectrometry-based Proteomics Laboratories. *Journal of proteome research* **20**, 2010-2013,
1185 doi:10.1021/acs.jproteome.0c00853 (2021).
1186 82 Wieczorek, S. *et al.* DAPAR & ProStaR: software to perform statistical analyses in quantitative
1187 discovery proteomics. *Bioinformatics (Oxford, England)* **33**, 135-136,
1188 doi:10.1093/bioinformatics/btw580 (2017).
1189 83 Pounds, S. & Cheng, C. Robust estimation of the false discovery rate. *Bioinformatics (Oxford,*
1190 *England)* **22**, 1979-1987, doi:10.1093/bioinformatics/btl328 (2006).
1191 84 Smyth, G. K. Linear models and empirical bayes methods for assessing differential expression
1192 in microarray experiments. *Statistical applications in genetics and molecular biology* **3**,
1193 Article3, doi:10.2202/1544-6115.1027 (2004).
1194 85 Giai Gianetto, Q. *et al.* Calibration plot for proteomics: A graphical tool to visually check the
1195 assumptions underlying FDR control in quantitative experiments. *Proteomics* **16**, 29-32,
1196 doi:10.1002/pmic.201500189 (2016).

1197

FIGURE 1

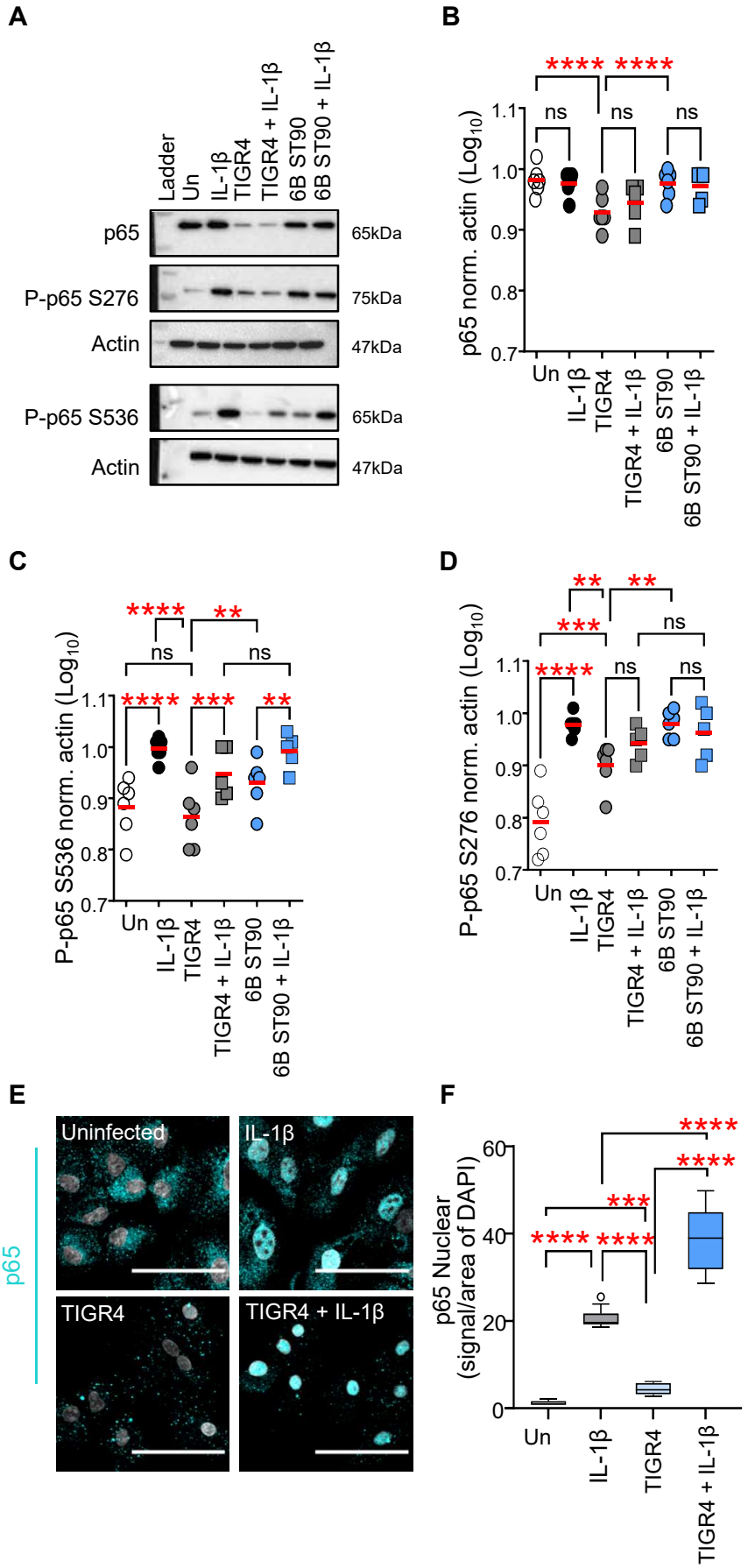
A
Ladder
Un
IL-1β
TIGR4
TIGR4 + IL-1β
6B ST90
6B ST90 + IL-1β
p65
P-p65 S276
Actin
P-p65 S536
Actin
65kDa
75kDa
47kDa
65kDa
47kDa
B
p65 norm. actin (Log10)
1.1
1.0
0.9
0.8
0.7
****
****
ns
ns
ns
Un
IL-1β
TIGR4
TIGR4 + IL-1β
6B ST90
6B ST90 + IL-1β
C
P-p65 S536 norm. actin (Log10)
1.1
1.0
0.9
0.8
0.7
****
**
ns
ns
****
***
**
Un
IL-1β
TIGR4
TIGR4 + IL-1β
6B ST90
6B ST90 + IL-1β
D
P-p65 S276 norm. actin (Log10)
1.1
1.0
0.9
0.8
0.7
**
**
***
ns
****
ns
ns
Un
IL-1β
TIGR4
TIGR4 + IL-1β
6B ST90
6B ST90 + IL-1β
E
p65
Uninfected
IL-1β
TIGR4
TIGR4 + IL-1β
F
p65 Nuclear
(signal/area of DAPI)
60
40
20
0
****
****
***
****
****
Un
IL-1β
TIGR4
TIGR4 + IL-1β

Sup. FIGURE 1

**A**

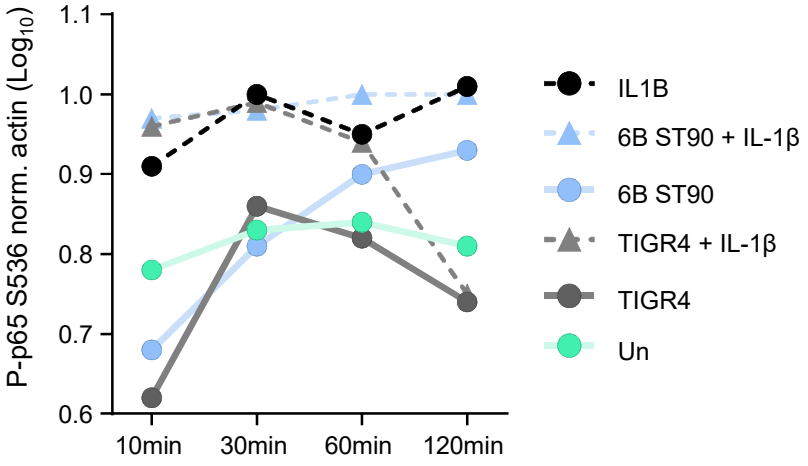


**B**

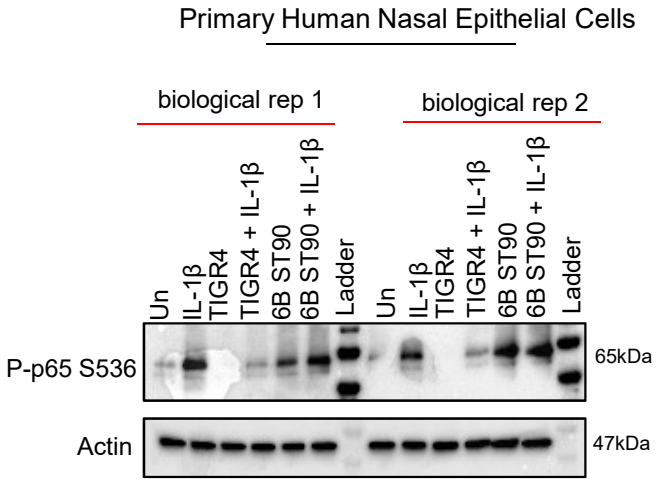


**C**

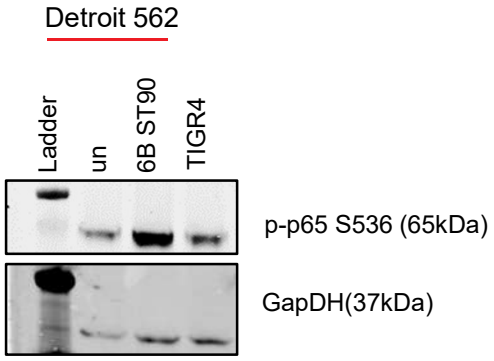


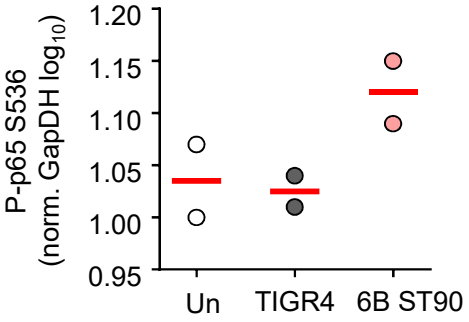

FIGURE 2

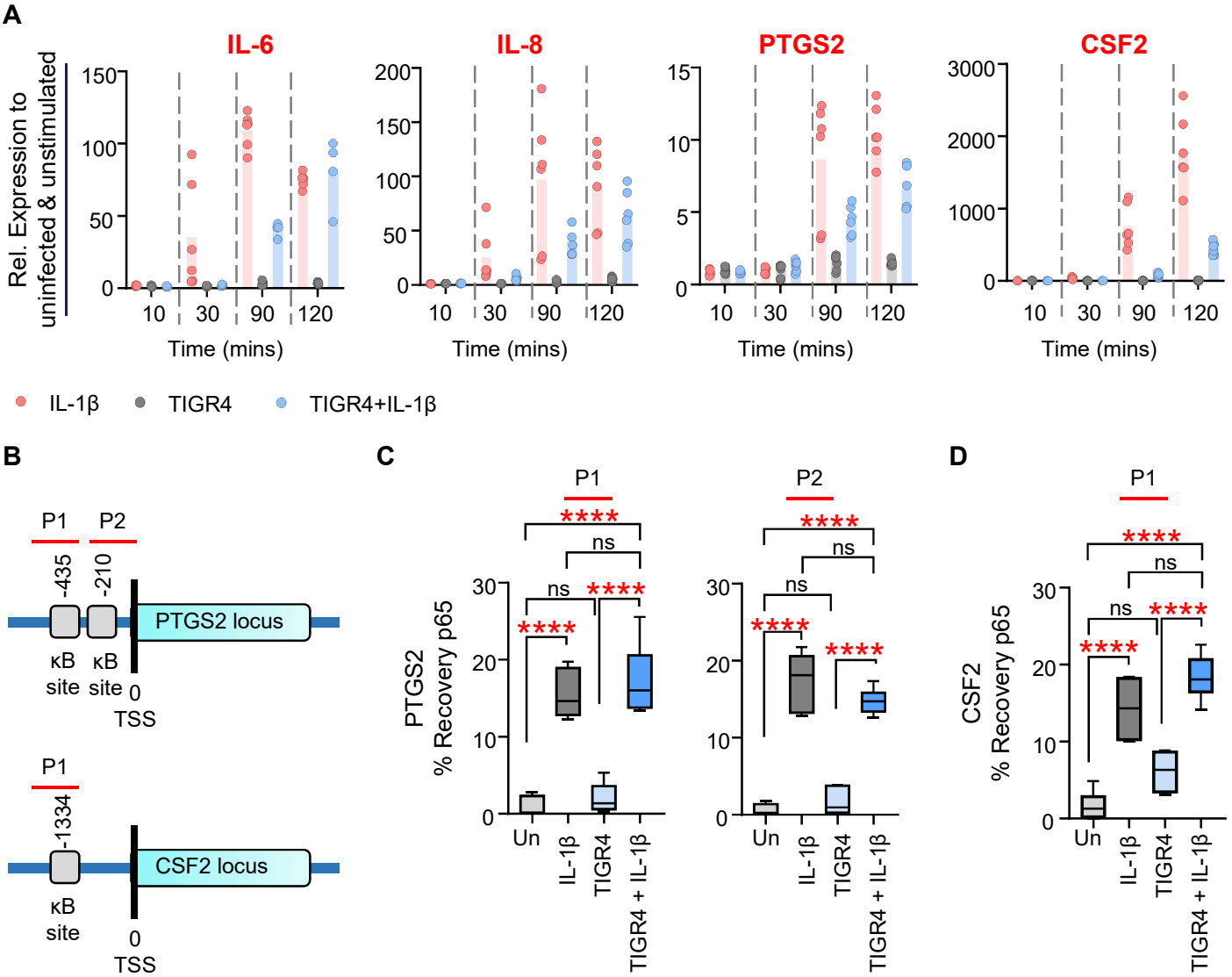
A
IL-6
IL-8
PTGS2
CSF2
Rel. Expression to uninfected & unstimulated
Time (mins)
IL-1β
TIGR4
TIGR4+IL-1β
B
P1
P2
-435
-210
PTGS2 locus
κB site
κB site
0
TSS
-1334
CSF2 locus
C
PTGS2 % Recovery p65
Un
IL-1β
TIGR4
TIGR4 + IL-1β
ns
****
D
CSF2 % Recovery p65

FIGURE 3

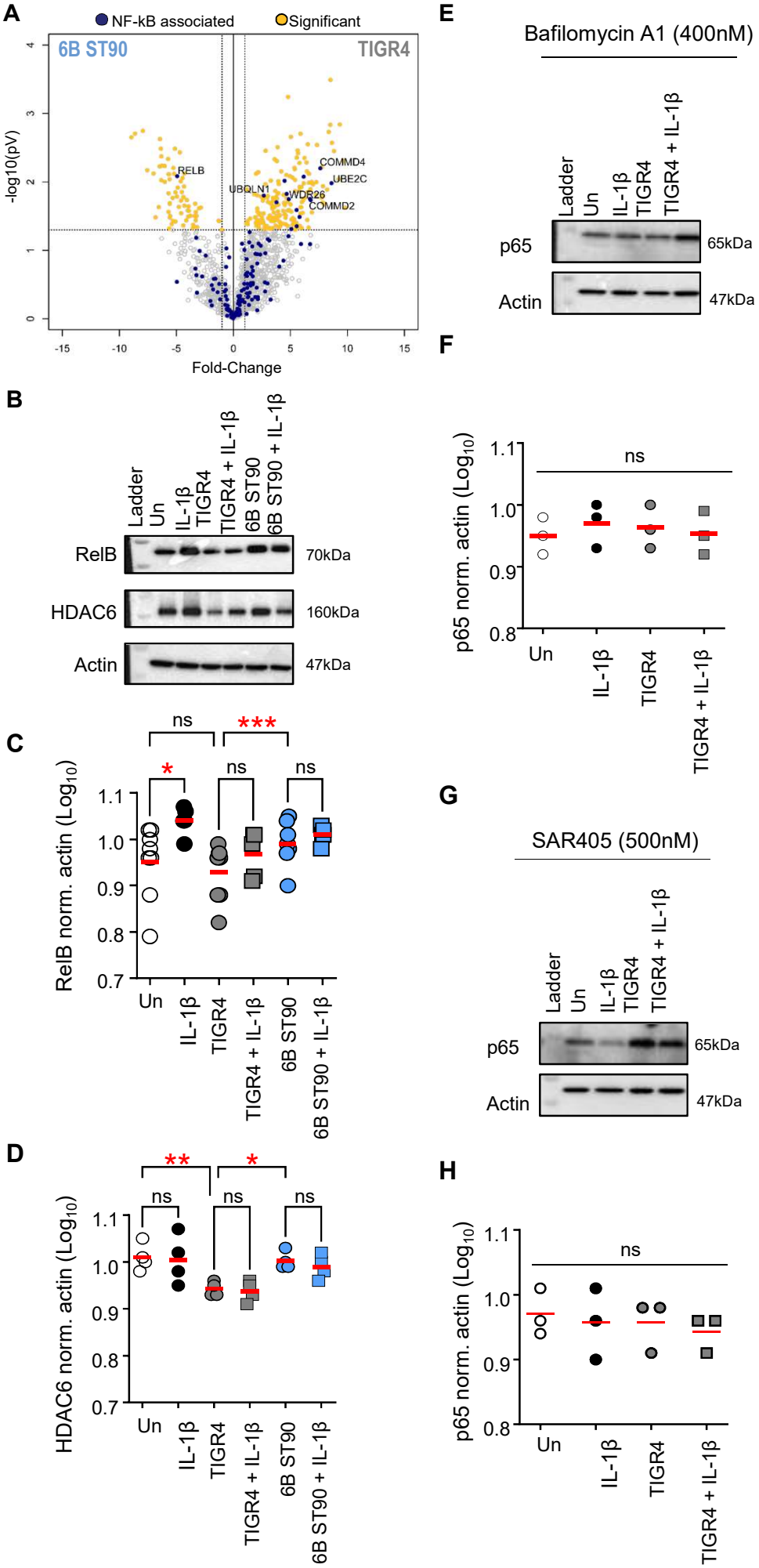
A
NF-kB associated
Significant
6B ST90
TIGR4
-log10(pV)
Fold-Change
RELB
UBQLN1
COMMD4
UBE2C
WDR26
COMMD2
B
Ladder
Un
IL-1β
TIGR4
TIGR4 + IL-1β
6B ST90
6B ST90 + IL-1β
RelB
HDAC6
Actin
70kDa
160kDa
47kDa
C
RelB norm. actin (Log10)
ns
***
*
ns
ns
Un
IL-1β
TIGR4
TIGR4 + IL-1β
6B ST90
6B ST90 + IL-1β
D
HDAC6 norm. actin (Log10)
**
*
ns
ns
ns
E
Bafilomycin A1 (400nM)
p65
65kDa
47kDa
F
p65 norm. actin (Log10)
ns
G
SAR405 (500nM)
H

Sup. FIGURE 2

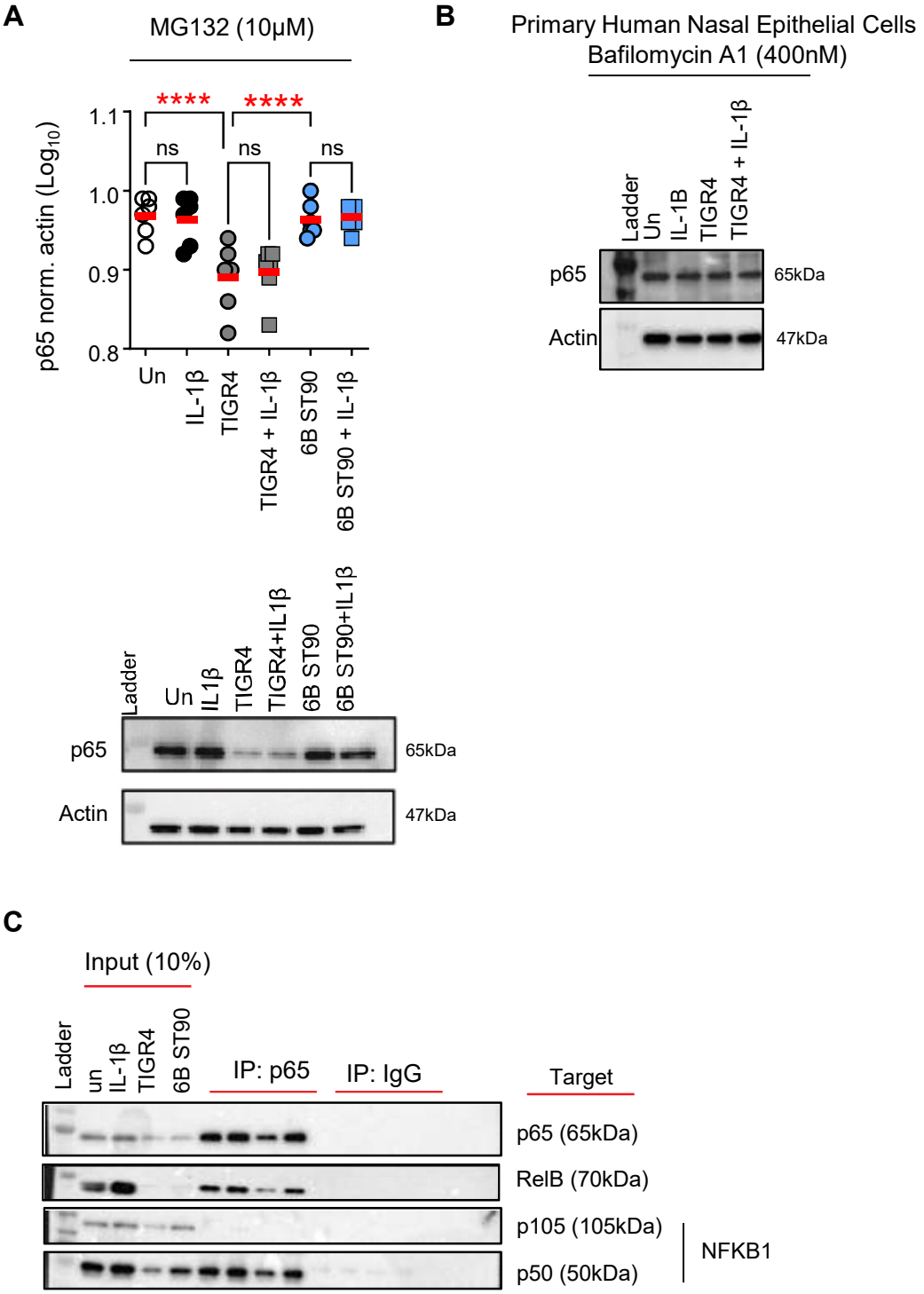
A
MG132 (10μM)
p65 norm. actin (Log10)
1.1
1.0
0.9
0.8
****
****
ns
ns
ns
Un
IL-1β
TIGR4
TIGR4 + IL-1β
6B ST90
6B ST90 + IL-1β
Ladder
Un
IL1β
TIGR4
TIGR4+IL1β
6B ST90
6B ST90+IL1β
p65
65kDa
Actin
47kDa
B
Primary Human Nasal Epithelial Cells
Bafilomycin A1 (400nM)
Ladder
Un
IL-1B
TIGR4
TIGR4 + IL-1β
p65
65kDa
Actin
47kDa
C
Input (10%)
Ladder
un
IL-1β
TIGR4
6B ST90
IP: p65
IP: IgG
Target
p65 (65kDa)
RelB (70kDa)
p105 (105kDa)
p50 (50kDa)
NFKB1

FIGURE 4

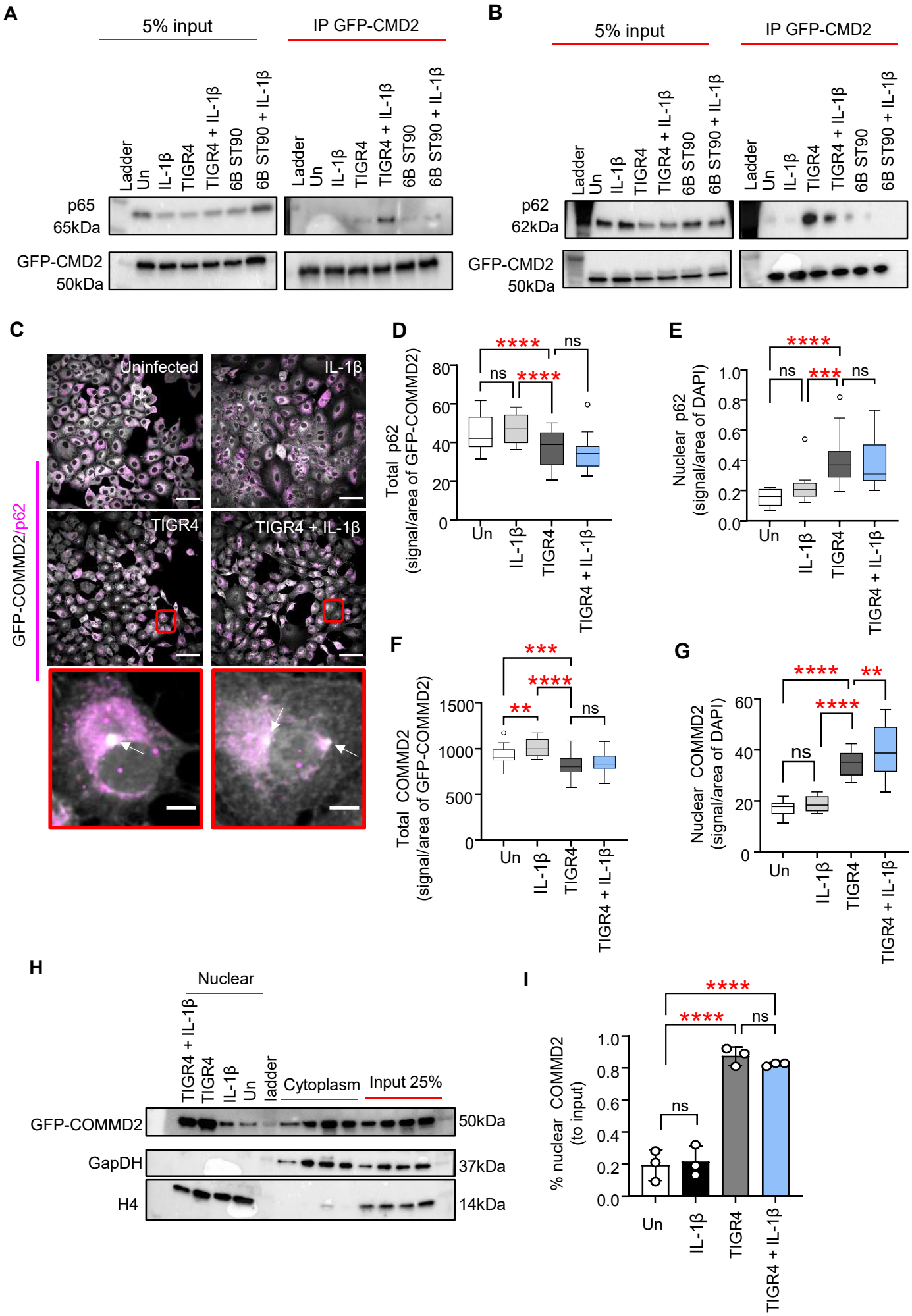
A
5% input
IP GFP-CMD2
Ladder
Un
IL-1β
TIGR4
TIGR4 + IL-1β
6B ST90
6B ST90 + IL-1β
p65
65kDa
GFP-CMD2
50kDa
B
p62
62kDa
C
Uninfected
IL-1β
TIGR4
TIGR4 + IL-1β
GFP-COMMD2/p62
D
Total p62 (signal/area of GFP-COMMD2)
E
Nuclear p62 (signal/area of DAPI)
F
Total COMMD2 (signal/area of GFP-COMMD2)
G
Nuclear COMMD2 (signal/area of DAPI)
H
Nuclear
Cytoplasm
Input 25%
GFP-COMMD2
GapDH
H4
50kDa
37kDa
14kDa
I
% nuclear COMMD2 (to input)

Sup. FIGURE 3

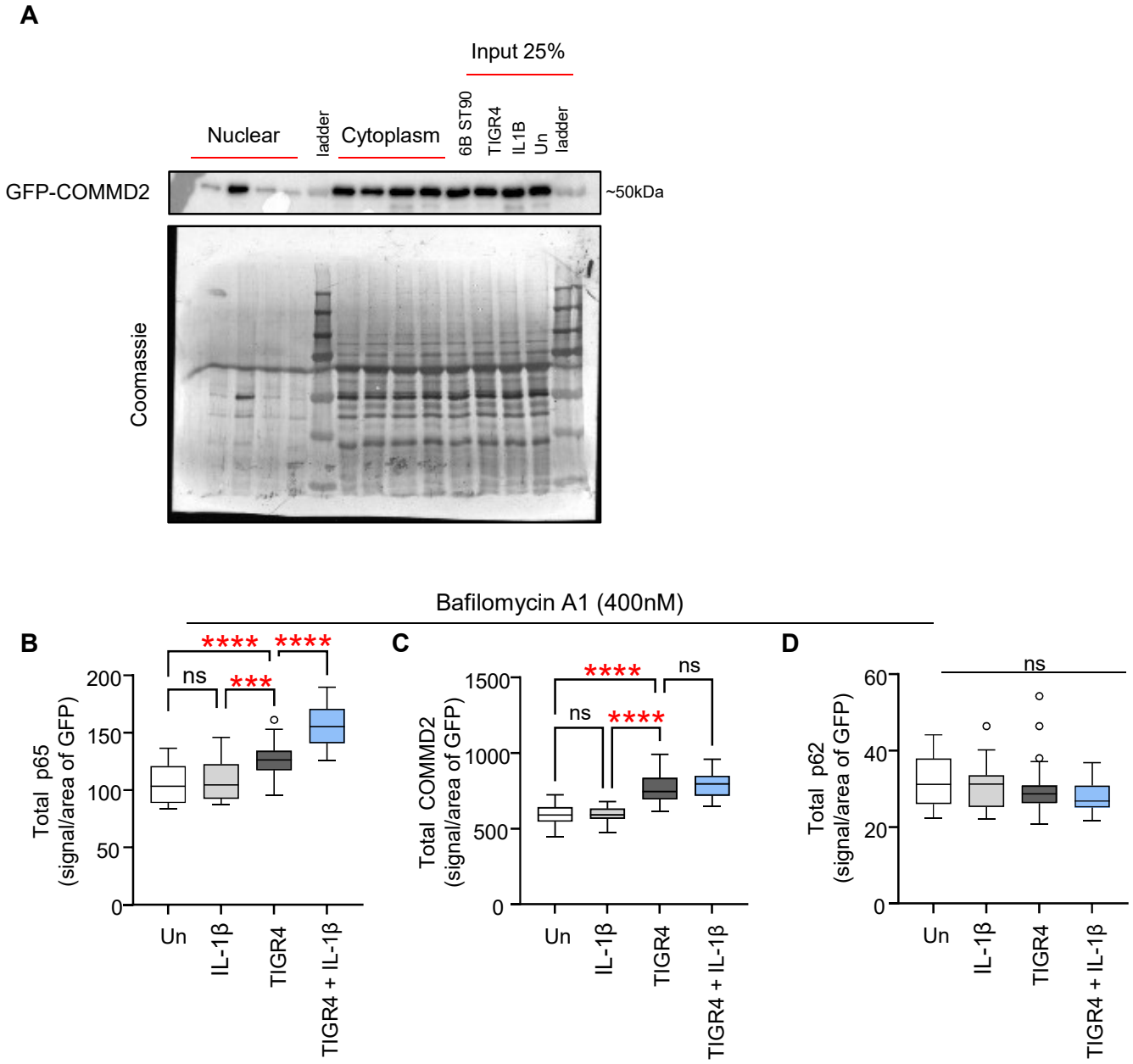
A
Input 25%
Nuclear
ladder
Cytoplasm
6B ST90
TIGR4
IL1B
Un
ladder
GFP-COMMD2
~50kDa
Coomassie
Bafilomycin A1 (400nM)
B
Total p65 (signal/area of GFP)
ns
***
****
****
Un
IL-1β
TIGR4
TIGR4 + IL-1β
C
Total COMMD2 (signal/area of GFP)
ns
****
****
ns
D
Total p62 (signal/area of GFP)
ns

FIGURE 5

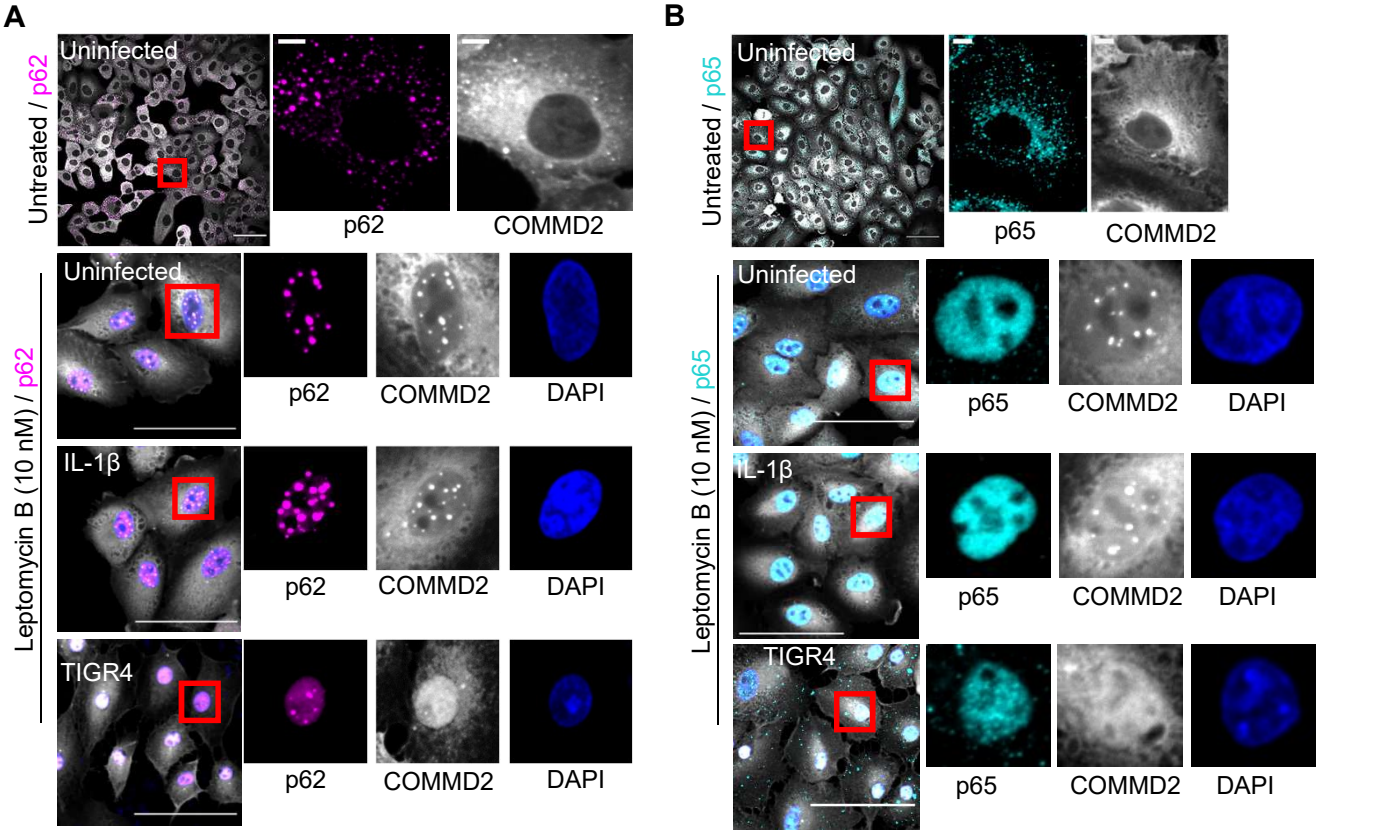
A
Untreated / p62
Uninfected
p62
COMMD2
Leptomycin B (10 nM) / p62
Uninfected
IL-1β
TIGR4
p62
COMMD2
DAPI
B
Untreated / p65
Uninfected
p65
COMMD2
Leptomycin B (10 nM) / p65
Uninfected
IL-1β
TIGR4
p65
COMMD2
DAPI

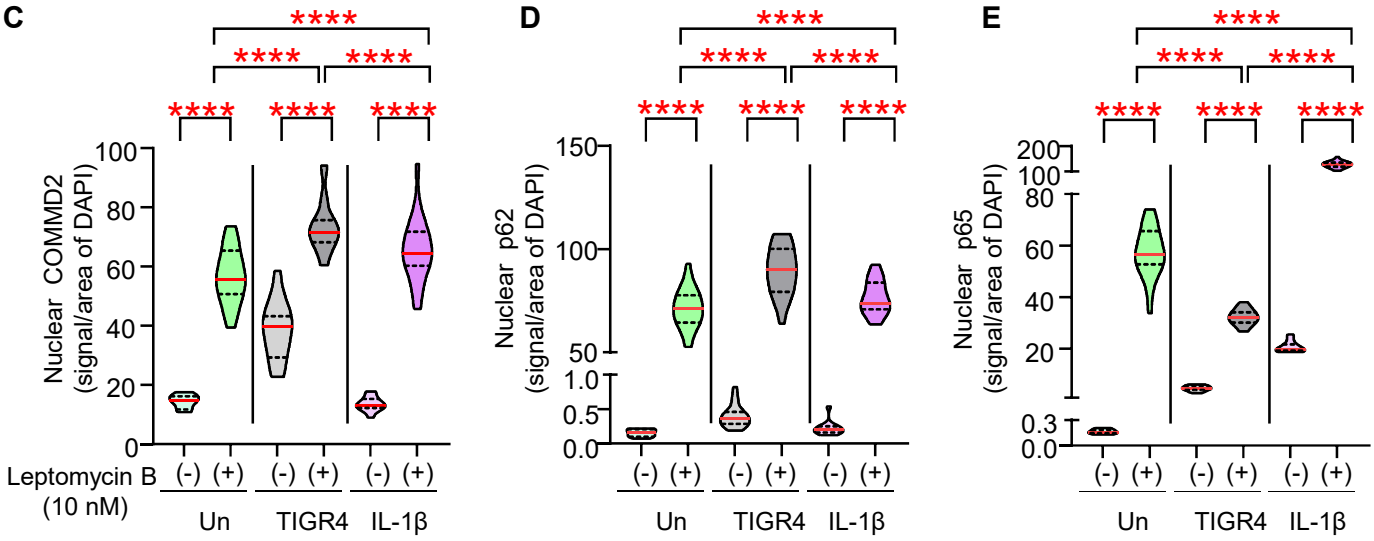
C
Nuclear COMMD2 (signal/area of DAPI)
D
Nuclear p62 (signal/area of DAPI)
E
Nuclear p65 (signal/area of DAPI)
****
Leptomycin B (10 nM)
(-) (+)
Un
TIGR4
IL-1β

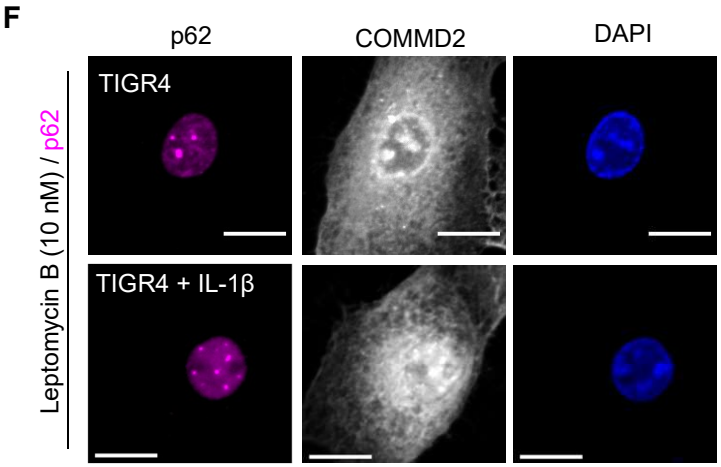
F
p62
COMMD2
DAPI
Leptomycin B (10 nM) / p62
TIGR4
TIGR4 + IL-1β

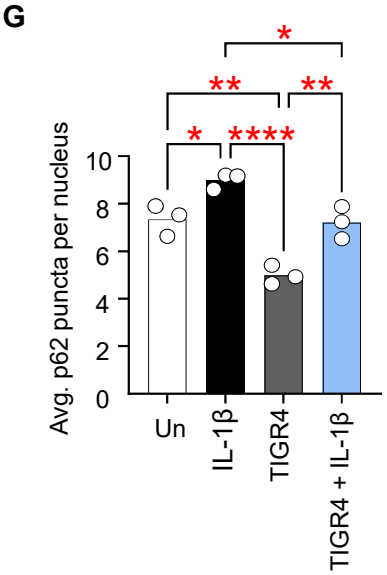
G
Avg. p62 puncta per nucleus
Un
IL-1β
TIGR4
TIGR4 + IL-1β

FIGURE 6

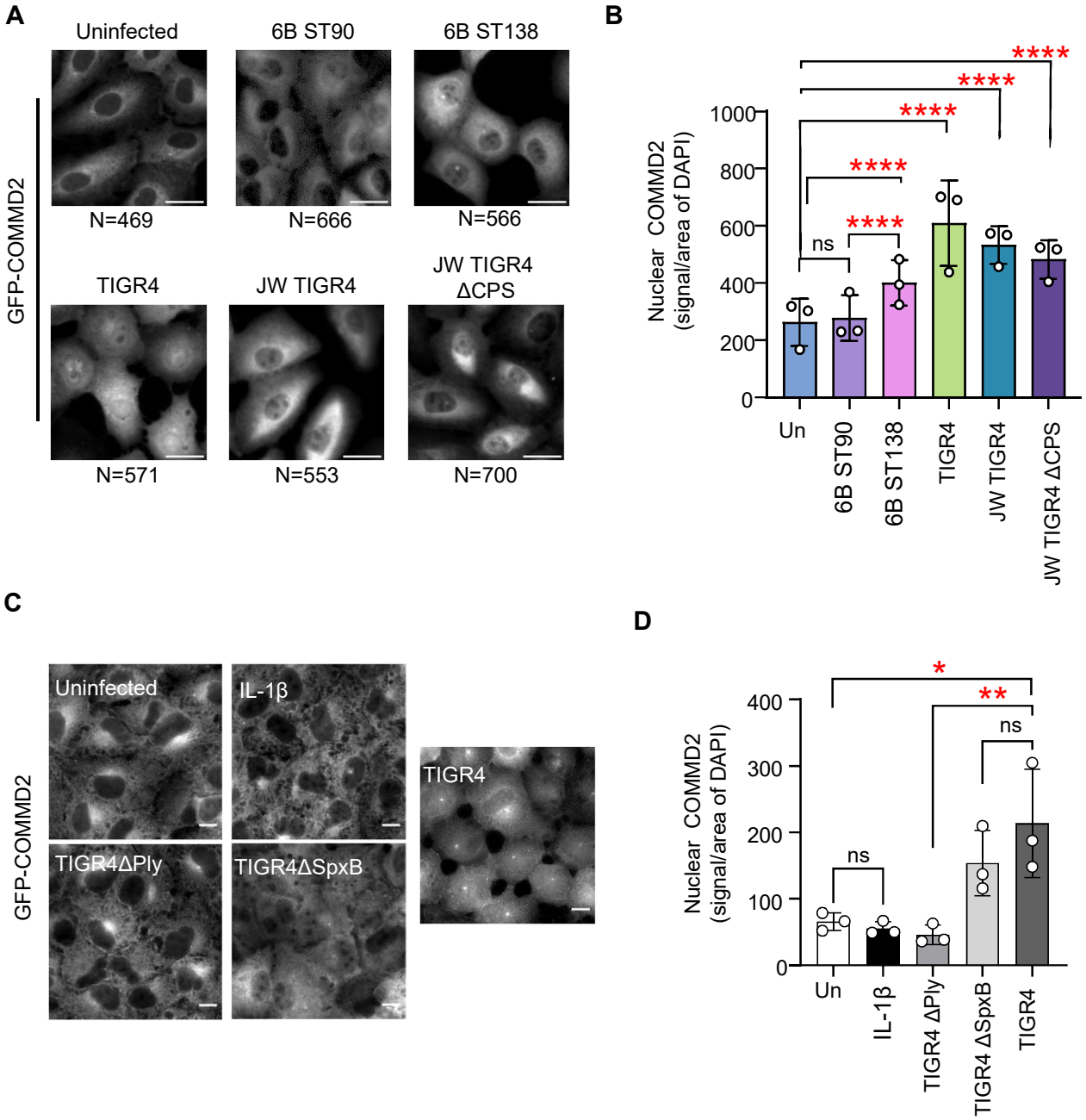
A
Uninfected
6B ST90
6B ST138
GFP-COMMD2
N=469
N=666
N=566
TIGR4
JW TIGR4
JW TIGR4 ΔCPS
N=571
N=553
N=700
B
Nuclear COMMD2 (signal/area of DAPI)
1000
800
600
400
200
0
****
ns
Un
6B ST90
6B ST138
TIGR4
JW TIGR4
JW TIGR4 ΔCPS
C
Uninfected
IL-1β
TIGR4
TIGR4ΔPly
TIGR4ΔSpxB
GFP-COMMD2
D
Nuclear COMMD2 (signal/area of DAPI)
400
300
200
100
0
*
**
ns
Un
IL-1β
TIGR4 ΔPly
TIGR4 ΔSpxB
TIGR4

FIGURE 7

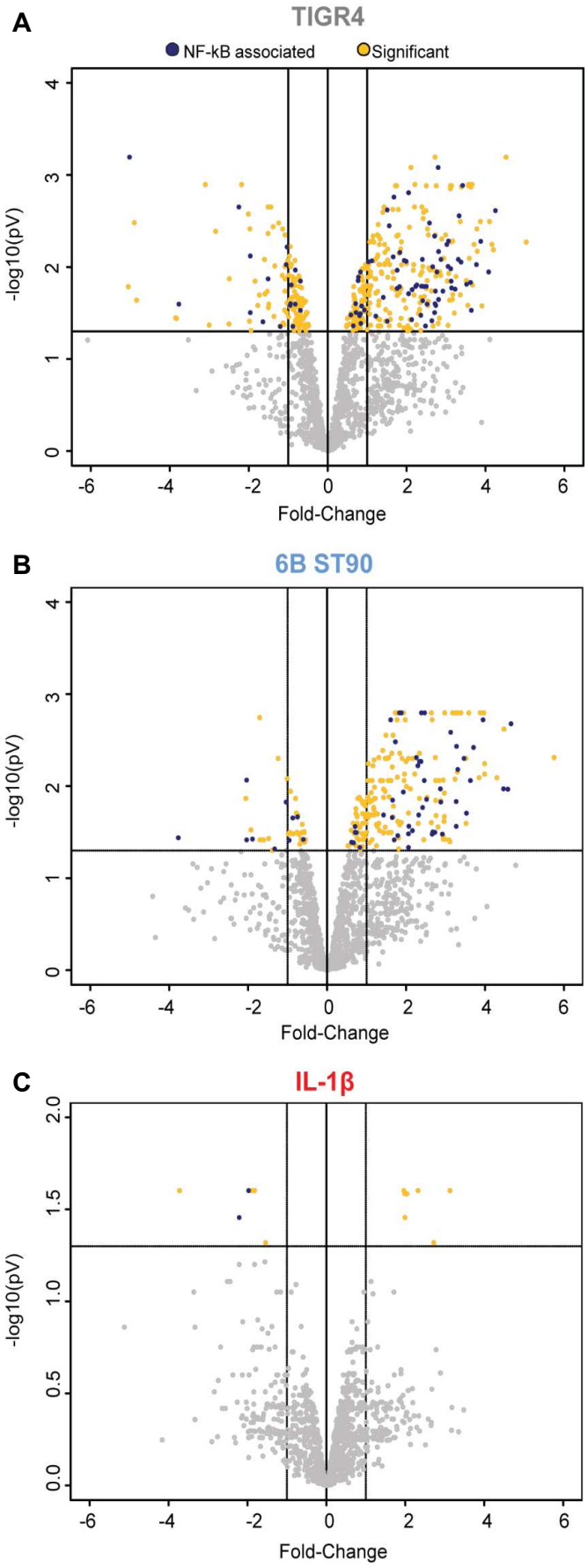


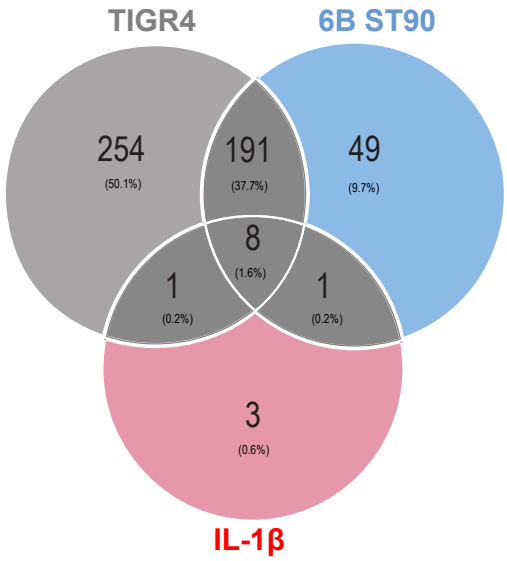


| | Significant vs. Un | Unique | Significant targets shared with p65 interactome |
|---|---|---|---|
| TIGR4 | 454 | 254 | 92 |
| 6B ST90 | 249 | 49 | 59 |
| IL-1β | 13 | 3 | - |

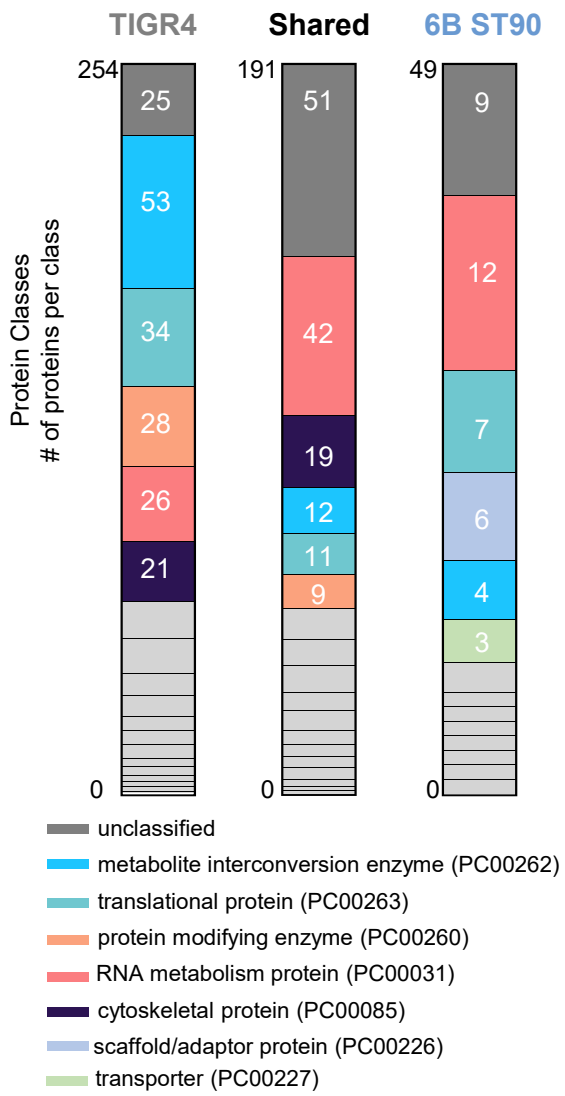

# FIGURE 8

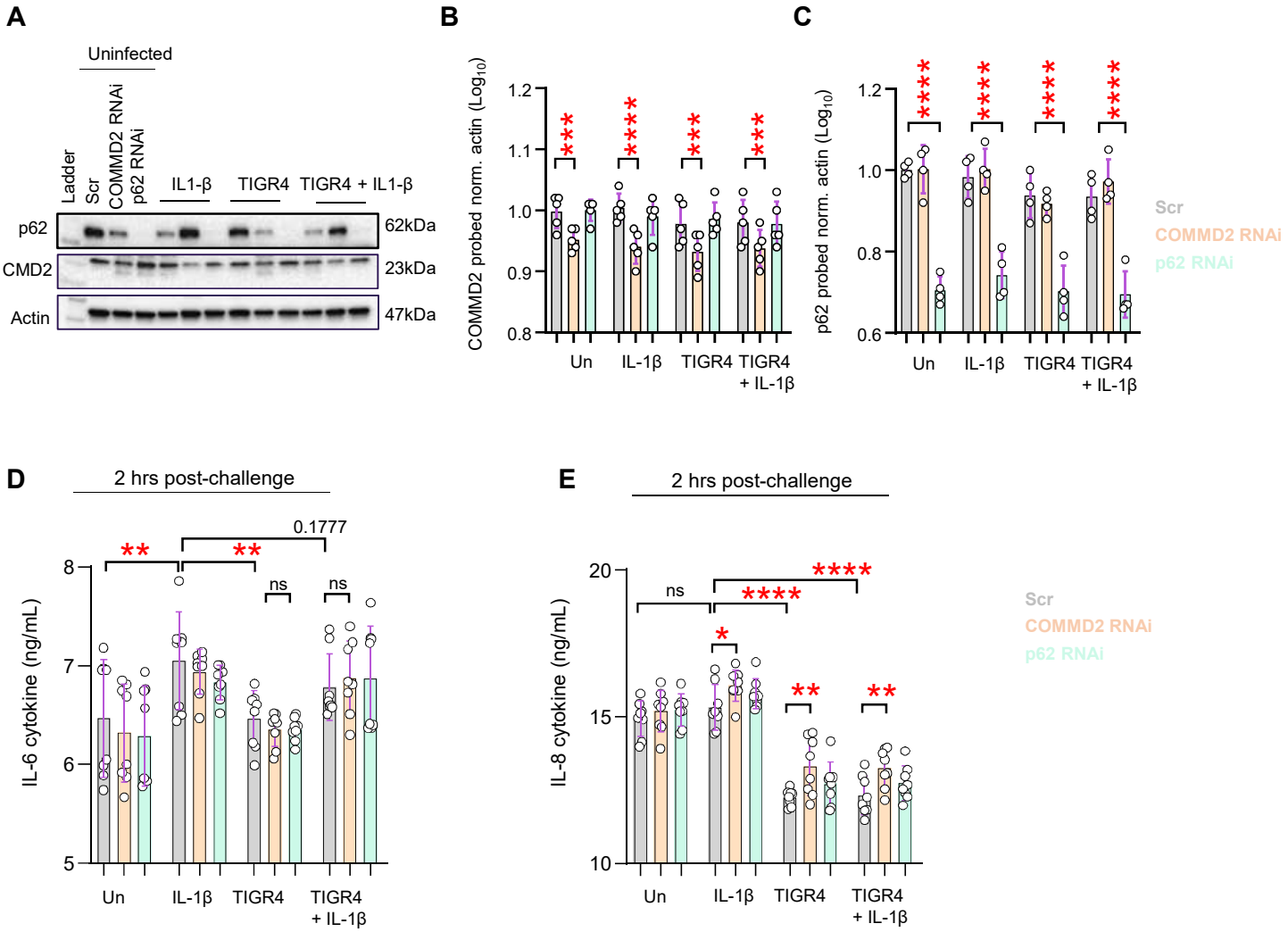
A
Uninfected
Ladder
Scr
COMMD2 RNAi
p62 RNAi
IL1-β
TIGR4
TIGR4 + IL1-β
p62
CMD2
Actin
62kDa
23kDa
47kDa
B
COMMD2 probed norm. actin (Log10)
1.2
1.1
1.0
0.9
0.8
Un
IL-1β
TIGR4
TIGR4 + IL-1β
C
p62 probed norm. actin (Log10)
1.2
1.0
0.8
0.6
Un
IL-1β
TIGR4
TIGR4 + IL-1β
Scr
COMMD2 RNAi
p62 RNAi
D
2 hrs post-challenge
IL-6 cytokine (ng/mL)
8
7
6
5
0.1777
ns
ns
Un
IL-1β
TIGR4
TIGR4 + IL-1β
E
2 hrs post-challenge
IL-8 cytokine (ng/mL)
20
15
10
ns
Un
IL-1β
TIGR4
TIGR4 + IL-1β
Scr
COMMD2 RNAi
p62 RNAi

# Sup. Information – Immunoblots Figure 1

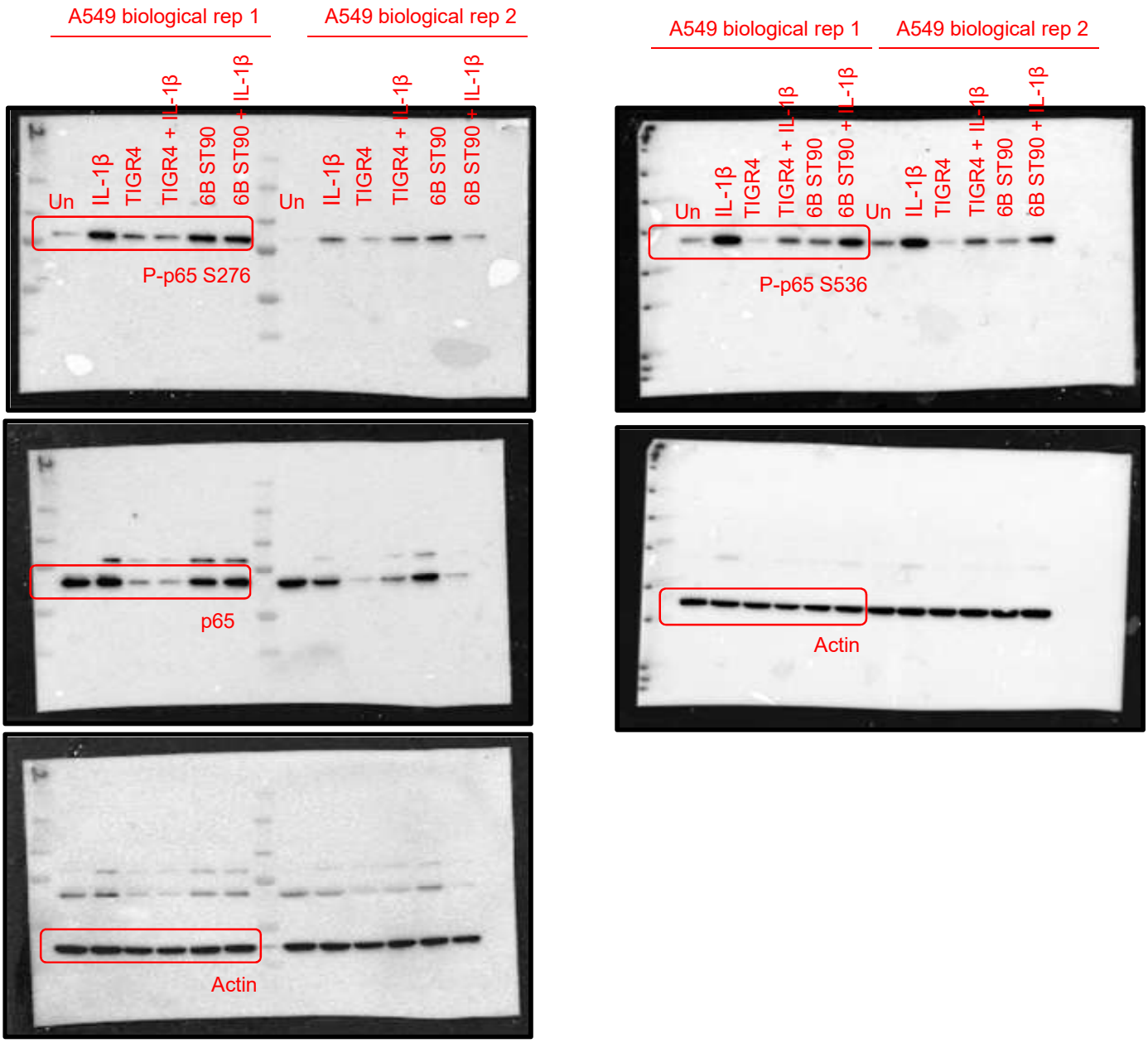

# Sup. Information – Immunoblots Figure 2

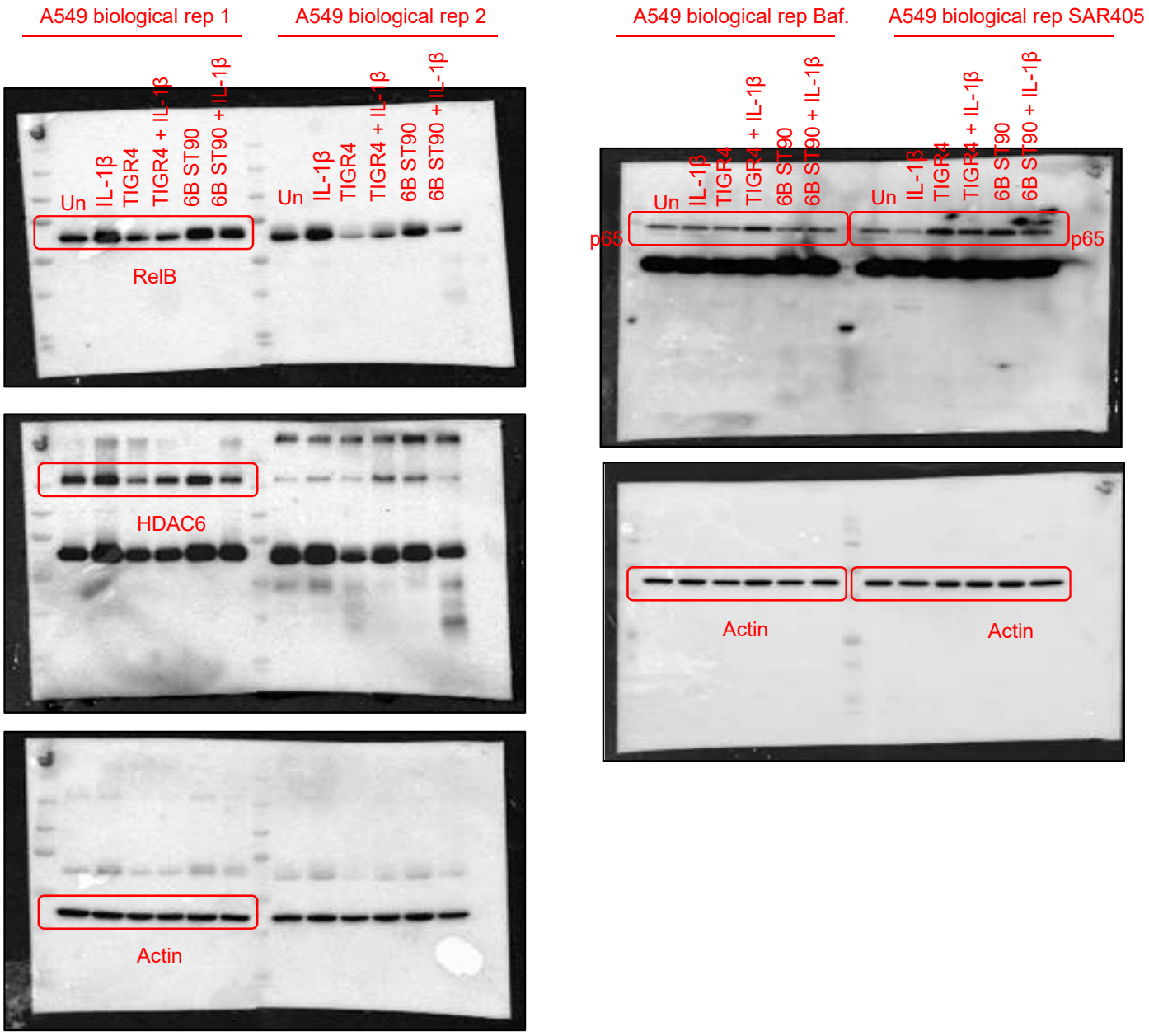

# Sup. Information – Immunoblots Figure 3

5% input

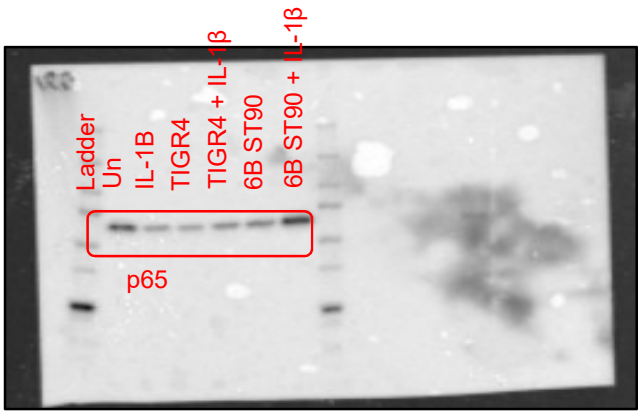


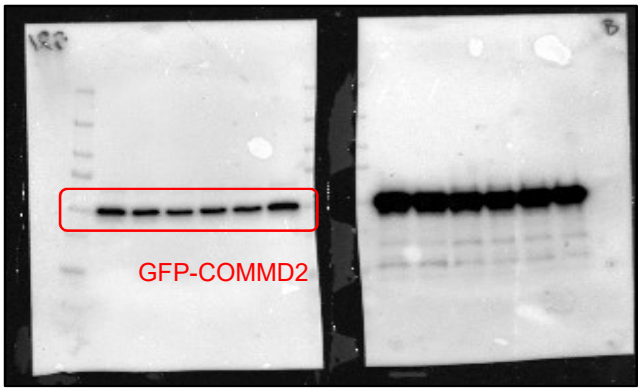


5% input

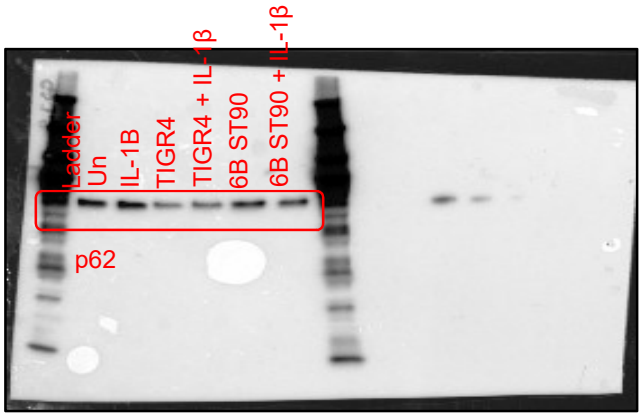


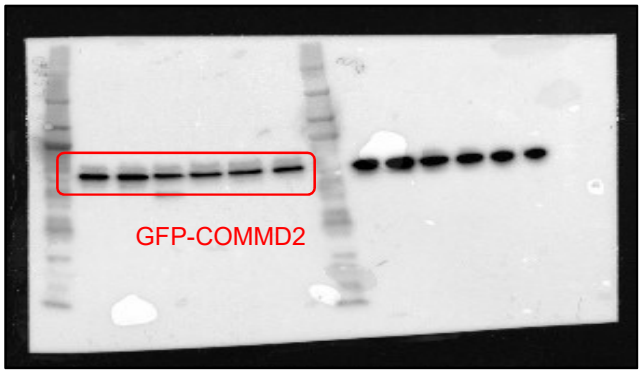


IP GFP-CMD2

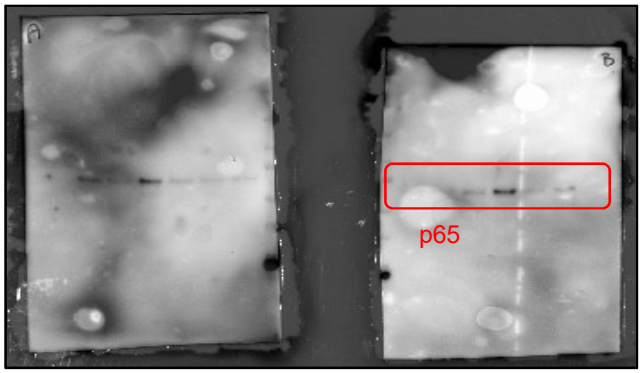


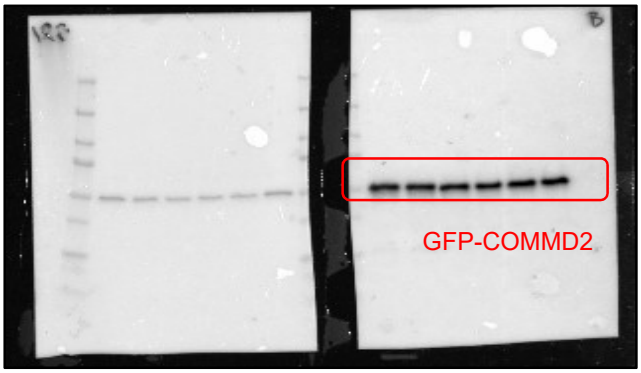


IP GFP-CMD2

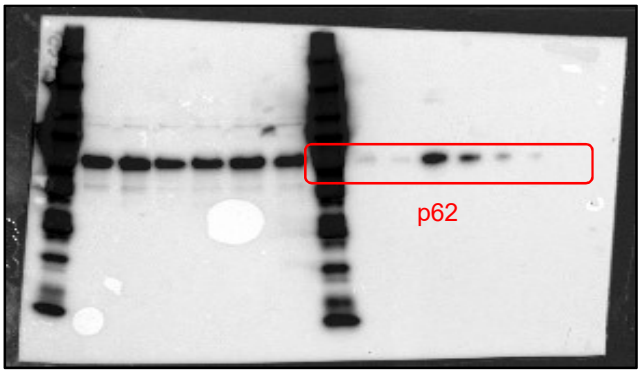


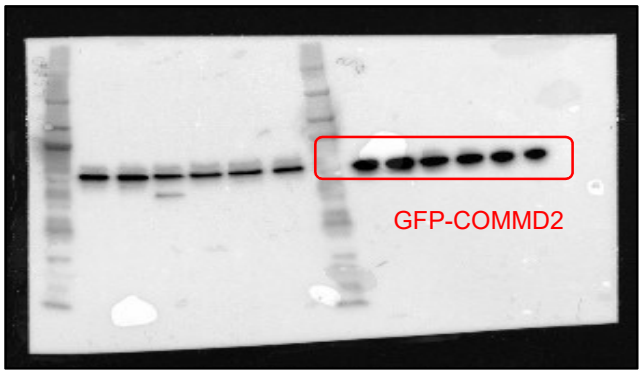

# Sup. Information – Immunoblots Figure 3 continued

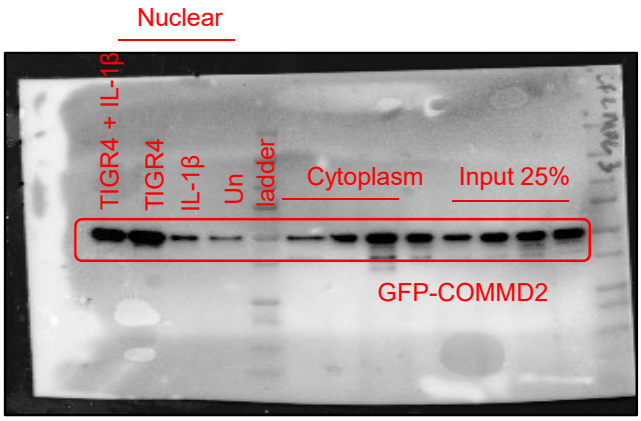


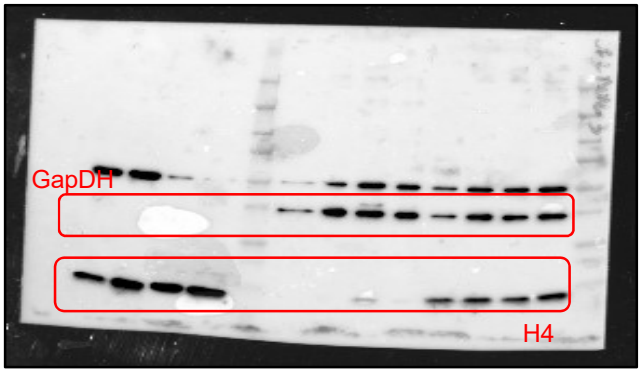

# Sup. Information – Immunoblots Figure 4
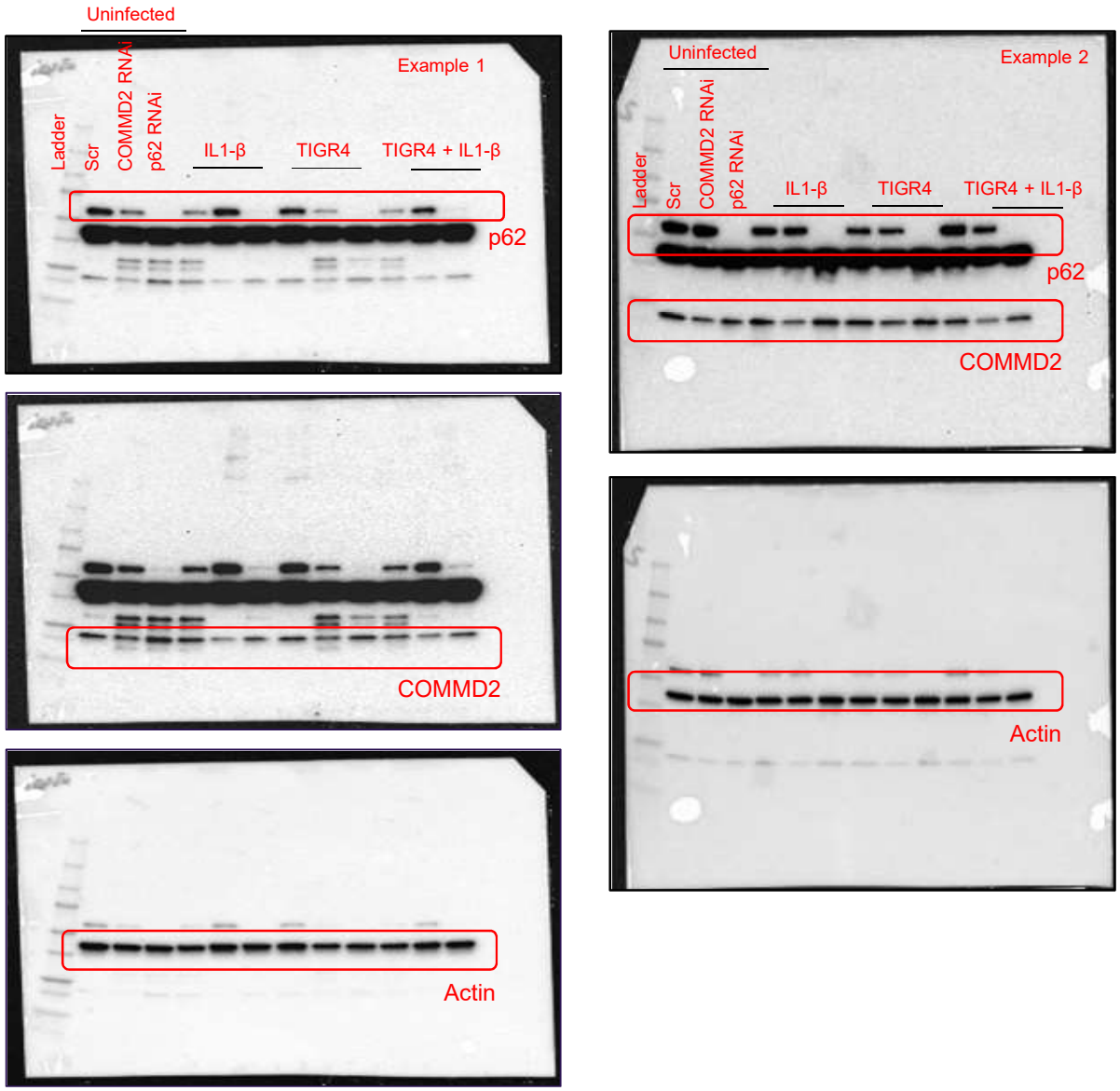
**A**